



HAL
open science

Comparison of the pharmacological properties of human and rat histamine H₃-receptors

David Schnell, Andrea Strasser, Roland Seifert

► **To cite this version:**

David Schnell, Andrea Strasser, Roland Seifert. Comparison of the pharmacological properties of human and rat histamine H₃-receptors. *Biochemical Pharmacology*, 2010, 80 (9), pp.1437. 10.1016/j.bcp.2010.07.027 . hal-00623303

HAL Id: hal-00623303

<https://hal.science/hal-00623303v1>

Submitted on 14 Sep 2011

HAL is a multi-disciplinary open access archive for the deposit and dissemination of scientific research documents, whether they are published or not. The documents may come from teaching and research institutions in France or abroad, or from public or private research centers.

L'archive ouverte pluridisciplinaire **HAL**, est destinée au dépôt et à la diffusion de documents scientifiques de niveau recherche, publiés ou non, émanant des établissements d'enseignement et de recherche français ou étrangers, des laboratoires publics ou privés.

Accepted Manuscript

Title: Comparison of the pharmacological properties of human and rat histamine H3-receptors

Authors: David Schnell, Andrea Strasser, Roland Seifert

PII: S0006-2952(10)00565-4
DOI: doi:10.1016/j.bcp.2010.07.027
Reference: BCP 10660

To appear in: *BCP*

Received date: 18-5-2010
Revised date: 20-7-2010
Accepted date: 23-7-2010

Please cite this article as: Schnell D, Strasser A, Seifert R, Comparison of the pharmacological properties of human and rat histamine H3-receptors, *Biochemical Pharmacology* (2010), doi:10.1016/j.bcp.2010.07.027

This is a PDF file of an unedited manuscript that has been accepted for publication. As a service to our customers we are providing this early version of the manuscript. The manuscript will undergo copyediting, typesetting, and review of the resulting proof before it is published in its final form. Please note that during the production process errors may be discovered which could affect the content, and all legal disclaimers that apply to the journal pertain.



Comparison of the pharmacological properties of human and rat histamine H₃-receptors

David Schnell, Andrea Strasser and Roland Seifert

Department of Pharmacology and Toxicology, University of Regensburg,

D-93040 Regensburg, Germany (D. S.)

Department of Pharmaceutical/Medicinal Chemistry I, University of Regensburg,

D-93040 Regensburg, Germany (A. S.)

Institute of Pharmacology, Medical School of Hannover,

D-30625 Hannover, Germany (R. S.)

Corresponding author:

Dr. Roland Seifert, Institute for Pharmacology, Medical School of Hannover, Carl-Neuberg-
Str. 1, D-30625 Hannover, Germany; Phone: +49-511-532-2805; Fax: +49-511-532-4081; e-
mail, seifert.roland@mh-hannover.de

Classification: Neuropharmacology

Abbreviations used: GPCR, G protein-coupled receptor; GTP γ S, guanosine 5'-[γ -thio]triphosphate; h, human; r, rat; β_2 AR, β_2 -adrenoceptor; H₃R, histamine H₃-receptor, H₄R, histamine H₄-receptor; TM, transmembrane domain; JNJ-7753707, (4-fluorophenyl)(1-methyl-2-an-1*H*-imidazol-5-yl)methanone; FUB181, 4-(3-(3-(4-chlorophenyl)propoxy)propyl)-1*H*-imidazole; A-304121, (*R*)-2-amino-1-(4-(3-(4-(cyclopropanecarbonyl)phenoxy)-propyl)piperazin-1-yl)propan-1-one; fMLP, N-formyl-L-methionyl-L-leucyl-L-phenylalanine; THIO, thioperamide

ABSTRACT

1
2 Ligand pharmacology of histamine H₃-receptors is species-dependent. In previous studies,
3
4 two amino acids in transmembrane domain 3 (TM III) were shown to play a significant role. In
5
6 this study, we characterized human and rat histamine H₃-receptors (hH₃R and rH₃R,
7
8 respectively), co-expressed with mammalian G proteins in Sf9 insect cell membranes. We
9
10 compared a series of imidazole-containing H₃R ligands in radioligand binding and steady-
11
12 state GTPase assays. H₃R_s similarly coupled to G $\alpha_{i/o}$ -proteins. Affinities and potencies of the
13
14 agonists histamine, *N*^H-methylhistamine and *R*-(α)-methylhistamine were in the same range.
15
16 Imetit was only a partial agonist. The pharmacology of imetit and proxifan was similar at both
17
18 species. However, impentamine was more potent and efficacious at rH₃R. The inverse
19
20 agonists ciproxifan and thioperamide showed higher potency but lower efficacy at rH₃R.
21
22 Clobenpropit was not species-selective. Strikingly, imoproxifan was almost full agonist at
23
24 hH₃R, but an inverse agonist at rH₃R. Imoproxifan was docked into the binding pocket of
25
26 inactive and active hH₃R- and rH₃R-models and molecular dynamic simulations were
27
28 performed. Imoproxifan bound to hH₃R and rH₃R in *E*-configuration, which represents the
29
30 *trans*-isomer of the oxime-moiety as determined in crystallization studies, and stabilized
31
32 active hH₃R-, but inactive rH₃R-conformations. Large differences in electrostatic surfaces
33
34 between TM III and TM V cause differential orientation of the oxime-moiety of imoproxifan,
35
36 which then differently interacts with the rotamer toggle switch Trp^{6.48} in TM VI. Collectively,
37
38 the substantial species differences at H₃R_s are explained at a molecular level by the use of
39
40 novel H₃R active-state models.
41
42
43
44
45
46
47
48

49 Key words: active receptor state; histamine H₃-receptor; imoproxifan; molecular dynamics
50
51 simulations; Sf9 insect cells
52
53
54
55
56
57
58
59
60
61
62
63
64
65

1. INTRODUCTION

1
2 Histamine (HA) exhibits its biological effects through the activation of four different G
3 protein-coupled receptors (GPCRs). The histamine H₁-receptor (H₁R) is associated with
4 inflammatory and allergic reactions, e. g. it increases vascular permeability and NO
5 production [1]. The histamine H₂-receptor (H₂R) regulates gastric acid production, but also
6 shows a positive inotropic effect on the heart [1]. The histamine H₃-receptor (H₃R) is a
7 presynaptic auto- and heteroreceptor, regulating the release of HA and various other
8 neurotransmitters in the nervous system, and is involved in important physiological
9 processes like the sleep-wake cycle, eating behaviour and cognition [2]. The histamine H₄-
10 receptor (H₄R) mediates inflammatory and immunological processes, e. g. chemotaxis of
11 eosinophils, mast cells and dendritic cells, but it is also present on neurons mediating HA-
12 induced itching [3, 4]. H₁R and H₂R antagonists have been used as therapeutics for decades,
13 H₃R and H₄R are still explored and promising new drug targets [5].

14
15 The H₃R was pharmacologically identified in the early 1980s, but cloned almost 20
16 years later in 1999 as an orphan GPCR [2]. The reason for this delay was that it only shares
17 ~20% homology to the H₁R and H₂R. The complex gene structure of the human H₃R (hH₃R)
18 gives rise to many possible splice variants. To date about 20 hH₃R splice variants are known
19 [6], but their function still remains elusive. The H₃R displays high constitutive, i. e. ligand-
20 independent, activity in many experimental systems [7]. The H₃R is one of the very few
21 GPCRs for which constitutive activity has also been demonstrated *in vivo* [8].

22
23 For the H₃R it has also been shown that species-differences exist [9, 10]. Fig. 1
24 shows the amino acid sequences of hH₃R and rH₃R. Although the H₃R sequence has a high
25 degree of similarity among species, differences located in key regions of the receptor protein
26 account for differences in antagonist affinity [13, 14]. Additionally, splice variants differ in
27 composition and expression pattern between species, and there are potential differences in
28 signal transduction processes between either tissues and/or species [15]. Nevertheless,
29 there are still unresolved questions about species differences of the full-length and un-
30
31
32
33
34
35
36
37
38
39
40
41
42
43
44
45
46
47
48
49
50
51
52
53
54
55
56
57
58
59
60
61
62
63
64
65

1
2
3
4
5
6
7
8
9
10
11
12
13
14
15
16
17
18
19
20
21
22
23
24
25
26
27
28
29
30
31
32
33
34
35
36
37
38
39
40
41
42
43
44
45
46
47
48
49
50
51
52
53
54
55
56
57
58
59
60
61
62
63
64
65

spliced H₃Rs (445 amino acids), especially regarding the detailed molecular mechanisms involved in ligand-receptor interactions.

In the present study, we systematically compared the pharmacological properties of hH₃R and rH₃R. Fig. 2 shows the structures of the compounds studied, all of them being imidazole-containing ligands. We co-expressed hH₃R and rH₃R in Sf9 cells together with mammalian G proteins in a defined stoichiometry, determined the affinity of ligands in radioligand binding studies, and their potency and efficacy in steady-state GTPase assays. The baculovirus/Sf9 cell system is very suitable for the analysis of G_i/G_o-coupled receptors and in particular constitutively active receptors, because in Sf9 cells no endogenous G_i/G_o-proteins or GPCRs with constitutive activity are present. The controlled expression of receptor and G proteins in Sf9 cell membranes represents more the physiological situation than, for example, the construction of GPCR-G α fusion proteins, because fusion proteins do not exist physiologically and the mobility of the G proteins is not restricted in the co-expression system. Moreover, the use of very proximal read-outs, like radioligand binding or steady-state GTPase assays prevent possible bias in later steps of the signal transduction cascade.

Many studies of ligand-receptor interactions come to a point where structural information on the atomic level is needed to explain experimental results. In the case of GPCRs, this is a very challenging and time-consuming process, and at the end only snapshots of static ligand-receptor complexes are resolved [16]. However, more and more high-resolution crystal structures of inactive- and active-state GPCR-ligand complexes are becoming available and can be used to generate better homology models [17, 18, 19]. Several molecular modelling studies with regard to ligand-receptor interaction at H₃R are found in literature [13, 20, 21, 22]. Since active-state models for H₃Rs do not yet exist, we generated and used those models to explain the pharmacological species differences at hH₃R and rH₃R on the basis of experimental data.

2. MATERIALS AND METHODS

2.1. Materials.

The cDNAs of the hH₃R and rH₃R were kindly provided by Dr. T. Lovenberg (Johnson & Johnson Pharmaceutical R&D, San Diego, CA, USA). An alignment of the corresponding amino acid sequences is given in Fig. 1. Anti-hH₃R Ig and anti-rH₃R Ig were from Bio-Trend (Cologne, Germany). The antibody recognizing both species homologs was from GeneWay (San Diego, CA, USA). All other antibodies, purified G proteins, reagents for molecular biology, recombinant baculoviruses encoding mammalian G protein subunits, and the sources of test compounds were described before [23]. Chemical structures of H₃R ligands are depicted in Fig. 2. Stock solutions (10 mM) of all H₃R ligands described in this paper were prepared in distilled water and stored at -20°C. [³H]JNJ-7753707 (= [³H]RWJ-422475) (30 Ci/mmol) was kindly donated from Dr. P. Bonaventure (Johnson & Johnson Pharmaceutical R&D, San Diego, CA, USA). [³H]N^α-methylhistamine (74-85 Ci/mmol) and [³⁵S]GTP_γS (1100 Ci/mmol) were obtained from Perkin Elmer (Boston, MA, USA). [^γ-³²P]GTP was synthesized as described [23]. Unlabeled nucleotides were from Roche (Indianapolis, IN, USA) and all other reagents were of the highest purity available and from standard suppliers.

2.2. Construction of FLAG epitope- and hexahistidine-tagged cDNAs for hH₃R and rH₃R.

The cDNA for the tagged rH₃R protein was generated by sequential overlap-extension PCR in analogy to the procedure described recently for hH₃R [23]. In the case of rH₃R, the sense primer RAT HRH3-F- (5'- GAC GAT GAT GAC GCC ATG GAG CGC GCG CCG CC-3') consisted of 15 bp of the 3'-end of SF and the first 17 bp of the 5'-end of the rH₃R. The antisense primer RAT HRH3-RV (5'- GA TCC TCT AGA TTA GTG ATG GTG ATG ATG GTG CTT CCA GCA CTG CTC -3') consisted of 15 bp of the C-terminus of the rH₃R, and encoded a hexahistidine tag, the *stop codon*, and a XbaI site. As template, a plasmid (pCIneo) containing the sequence of rH₃R was used.

2.3. Generation of recombinant baculoviruses, cell culture and membrane preparation, SDS-PAGE and immunoblot analysis.

The protocols for virus amplification, protein expression and western blot analysis were described before [23]. Proteins transferred to nitrocellulose membranes were reacted with anti-hH₃R (N-term) (1:1000), anti-rH₃R (C-term) (1:1000) and anti-H₃R (i3) (1:1000) Igs.

2.4. [³⁵S]GTP_γS saturation binding assay.

Experiments were performed in analogy to the assay described in Schnell et al. [23].

Membranes were thawed and sedimented by a 10-min centrifugation at 4°C and 15,000g to remove residual endogenous guanine nucleotides as far as possible. Membranes were resuspended in binding buffer (12.5 mM MgCl₂, 1 mM EDTA, and 75 mM Tris-HCl, pH 7.4), supplemented with 0.05% (m/v) BSA. Each tube (total volume of 250 or 500 μl) contained 10 - 20 μg of membrane protein. Tubes contained 0.2 – 2 nM [³⁵S]GTP_γS plus unlabeled GTP_γS to give the desired final ligand concentrations (0.2 – 50 nM). Neither GDP nor H₃R ligands were included in assays. Non-specific binding was determined in the presence of 100 μM unlabeled GTP_γS and amounted to less than 1% of total binding. Incubations were conducted for 90 minutes at 25°C and shaking at 250 rpm. Bound [³⁵S]GTP_γS was separated from free [³⁵S]GTP_γS by filtration through GF/C filters, followed by three washes with 2 ml of binding buffer (4°C). Filter-bound radioactivity was determined by liquid scintillation counting. The experimental conditions chosen ensured that not more than 10 % of the total amount of radioactivity added to binding tubes was bound to filters. The maximum number of G_{α_{i/o}}-related GTP_γS binding sites in membranes expressing H₃Rs plus G_α-subunits plus β₁γ₂ was corrected by the binding determined in parallel in membranes expressing H₃Rs plus β₁γ₂ alone. These reference membranes were always prepared under exactly the same conditions as the other ones. To ensure the same viral load in the reference membranes, Sf9 cells were infected with baculoviruses encoding H₃Rs, β₁γ₂ and virus encoding no recombinant protein at all. In this manner, only the number of functionally intact and heterologously expressed mammalian G_{α_{i/o}}-subunits was quantitated.

2.5. Steady-state GTPase activity assay.

1
2 Experiments were performed in analogy to the assay described in Schnell et al. [23]. Briefly,
3 membranes were thawed, sedimented and resuspended in 10 mM Tris/HCl, pH 7.4. Assay
4 tubes contained Sf9 membranes (10 – 20 µg of protein/tube), 5.0 mM MgCl₂, 0.1 mM EDTA,
5
6
7
8
9
10
11
12
13
14
15
16
17
18
19
20
21
22
23
24
25
26
27
28
29
30
31
32
33
34
35
36
37
38
39
40
41
42
43
44
45
46
47
48
49
50
51
52
53
54
55
56
57
58
59
60
61
62
63
64
65

Experiments were performed in analogy to the assay described in Schnell et al. [23]. Briefly, membranes were thawed, sedimented and resuspended in 10 mM Tris/HCl, pH 7.4. Assay tubes contained Sf9 membranes (10 – 20 µg of protein/tube), 5.0 mM MgCl₂, 0.1 mM EDTA, 0.1 mM ATP, 100 nM GTP, 0.1 mM adenylyl imidodiphosphate, 1.2 mM creatine phosphate, 1 µg of creatine kinase, and 0.2% (w/v) bovine serum albumin in 50 mM Tris/HCl, pH 7.4, and H₃R ligands at various concentrations. Reaction mixtures (80 µl) were incubated for 2 min at 25°C before the addition of 20 µl of [γ -³²P]GTP (0.1 µCi/tube). All stock and work dilutions of [γ -³²P]GTP were prepared in 20 mM Tris/HCl, pH 7.4. Reactions were conducted for 20 min at 25°C. Reactions were terminated by the addition of 900 µl of slurry consisting of 5% (w/v) activated charcoal and 50 mM NaH₂PO₄, pH 2.0. Charcoal absorbs nucleotides but not P_i. Charcoal-quenched reaction mixtures were centrifuged for 7 min at room temperature at 15,000g. Six hundred microliters of the supernatant fluid of reaction mixtures were removed, and ³²P_i was determined by liquid scintillation counting. Enzyme activities were corrected for spontaneous degradation of [γ -³²P]GTP. Spontaneous [γ -³²P]GTP degradation was determined in tubes containing all of the above described components plus a very high concentration of unlabeled GTP (1 mM) that, by competition with [γ -³²P]GTP, prevents [γ -³²P]GTP hydrolysis by enzymatic activities present in Sf9 membranes. Spontaneous [γ -³²P]GTP degradation was <1% of the total amount of radioactivity added using 20 mM Tris/HCl, pH 7.4, as solvent for [γ -³²P]GTP. The experimental conditions chosen ensured that not more than 10% of the total amount of [γ -³²P]GTP added was converted to ³²P_i.

2.6. Radioligand binding assays.

51 Experiments were performed in analogy to the assay described in Schnell et al. [23].
52
53
54
55
56
57
58
59
60
61
62
63
64
65

Experiments were performed in analogy to the assay described in Schnell et al. [23]. Membranes were thawed and sedimented by a 10-min centrifugation at 4°C and 15,000g and resuspended in binding buffer (12.5 mM MgCl₂, 1 mM EDTA, and 75 mM Tris-HCl, pH 7.4), to remove residual endogenous guanine nucleotides as much as possible. In [³H]NAMH binding assays, each tube (total volume, 250 or 500 µl) contained 10 to 50 µg of protein.

1
2
3
4
5
6
7
8
9
10
11
12
13
14
15
16
17
18
19
20
21
22
23
24
25
26
27
28
29
30
31
32
33
34
35
36
37
38
39
40
41
42
43
44
45
46
47
48
49
50
51
52
53
54
55
56
57
58
59
60
61
62
63
64
65

Non-specific binding was determined in the presence of [³H]NAMH at various concentrations plus 10 μM THIO and amounted to ~10% of total binding at saturating concentrations (10 nM). Incubations were conducted for 60 min at RT and shaking at 250 rpm. Saturation binding experiments were carried out using 0.3 to 10 nM [³H]NAMH in the presence or absence of 10 μM GTP_γS. In competition binding experiments, tubes contained 1 nM [³H]NAMH and unlabeled ligands at various concentrations. Bound [³H]NAMH was separated from free [³H]NAMH by filtration through GF/C filters pretreated with 0.3% (m/v) polyethyleneimine, followed by three washes with 2 ml of binding buffer (4°C). [³H]JNJ-7753707 (= [³H]RWJ-422475) binding experiments were performed using the same procedure as described above for [³H]NAMH. With [³H]JNJ-7753707 as radioligand, non-specific binding was about 20-30% of total binding at saturating concentrations (10 nM). Filter-bound radioactivity was determined by liquid scintillation counting. The experimental conditions chosen ensured that not more than 10 % of the total amount of radioactivity added to binding tubes was bound to filters.

2.7. Construction of inactive and active models of hH₃R and rH₃R.

Based on the crystal structure of the human β₂-adrenergic receptor [17, 24], a homology model of the inactive hH₃R and rH₃R were generated. Based on the active state model of guinea pig H₁R (gpH₁R) [25, 26], an active model of hH₃R was constructed by homology modelling. All models were refined and energetically minimized with SYBYL 7.0 (Tripos, St. Louis, MO, USA), as described [27]. Imoproxifan was docked manually into the binding pocket of the active hH₃R and the inactive rH₃R. Thereby, previous results of similar compounds were taken into account [20, 21]. The resulting structures were embedded in a simulation box, including lipid bilayer, water, sodium and chlorine ions, as described [28]. Subsequently, molecular dynamic simulations with GROMACS 3.3.1 [29] were performed, using a simulation protocol, previously described [28].

2.8. Miscellaneous.

1
2 Molecular biology was planned with GCK 2.5 (Textco BioSoftware, West Lebanon, NH,
3
4 USA). Ligand structures were illustrated using ChemDraw Ultra 8.0 (CambridgeSoft,
5
6 Cambridge, MA, USA). The sequence alignment was performed using ClustalX (2.0), which
7
8 is a windows interface based on the Clustal W algorithm [30]. Protein was determined using
9
10 the DC protein assay kit (Bio-Rad, Hercules, CA, USA). [³H]Dihydroalprenolol was obtained
11
12 from Perkin Elmer (Boston, MA, USA) and protein quantification via western blot performed
13
14 as described in Schnell et al. [23]. All analyses of experimental data were performed with the
15
16 Prism 5 program (GraphPad Software, San Diego, CA, USA).
17
18
19
20
21

3. RESULTS

3.1. Western blot analysis of hH₃R and rH₃R expressed in Sf9 insect cell membranes.

22
23
24
25
26 Membranes of Sf9 cells expressing hH₃R or rH₃R plus mammalian G proteins were prepared
27
28 and analyzed via immunoblot. It has to be mentioned, that membranes co-expressing rH₃R
29
30 plus different mammalian G proteins were prepared in parallel and under exactly the same
31
32 conditions as the membranes expressing hH₃R [23]. Thus, the comparison of hH₃R and rH₃R
33
34 pharmacology in this system is not based on historical data but direct. Both hH₃R and rH₃R
35
36 bands were doublets, probably representing differently glycosylated forms (Fig. 3). H₃R
37
38 species homologs presumably exhibit similar glycosylation patterns since the putative N-
39
40 glycosylation site for the H₃R (Asn11) is fully conserved within their sequences (Fig. 1). The
41
42 H₃R species homologs could be clearly discriminated by anti-hH₃R Ig, raised against an 18
43
44 amino acid peptide within the extracellular N-terminus of the hH₃R, and anti-rH₃R Ig, raised
45
46 against an 18 amino acid peptide within the cytoplasmatic C-terminus of the rH₃R (Figs. 3A
47
48 and 3B). Additionally, anti-H₃R (i3) Ig was used to confirm the above mentioned results (Fig.
49
50 and 3C). This antibody was raised against a peptide sequence within the third intracellular loop
51
52 (i3) of the hH₃R, but turned out to be not species-selective. Again, all H₃R bands occurred as
53
54 doublets at ~49 kDa. However, there were some additional bands at lower molecular weight,
55
56 which are presumably non-specific, since they also appeared at the control lane loaded with
57
58
59
60
61
62
63
64
65

1 uninfected Sf9 cell membranes. Thus, our data indicate that hH₃R and rH₃R were equally
2 well and properly expressed in Sf9 cells. In analogy to our recent publication [23], the rH₃R
3 was also co-expressed with different mammalian G proteins (G α_{i1} , G α_{i2} , G α_{i3} or G α_{o1} , and $\beta_1\gamma_2$
4 dimers, respectively) to analyze the coupling profile. All proteins were properly detected by
5 different selective antibodies (Fig. 3). Moreover, we also quantified the expression levels of
6 receptors and G proteins by immunoblot, using h β_2 AR or purified G protein subunits as
7 standards (Fig. 3D and 3H, I). The results of these studies are summarized in Table 1.
8
9

10 **3.2. Quantitative analysis of receptor-to-G protein stoichiometries.**

11 Protein quantification via western blot is semi-quantitative and does not discriminate between
12 functional and non-functional proteins. Therefore, we directly used a recently described
13 combination of antagonist [³H]JNJ-7753707- and [³⁵S]GTP γ S-saturation binding [23] and
14 calculated the functional GPCR/G α protein ratios (Table 1). Similar to the membranes
15 expressing hH₃R, we detected an excess of mammalian G proteins in the case of rH₃R,
16 confirming the previously reported results [23]. Thus, G protein expression level is not limiting
17 in this experimental system, too.
18
19

20 **3.3. hH₃R and rH₃R coupling to different G α -subunits.**

21 The G protein coupling profile of rH₃R (Table 2) was also investigated as for the hH₃R [23].
22 Briefly, receptor-dependent [γ -³²P]GTP hydrolysis of different G α -subunits was measured
23 under steady-state conditions. GTPase activities were determined in parallel under basal
24 conditions, maximal stimulation with the physiological (and full) agonist histamine (10 μ M)
25 and a saturating concentration of the inverse agonist thioperamide (10 μ M) in Sf9 cell
26 membranes co-expressing the rH₃R and different G proteins.
27
28

29 Like hH₃R, rH₃R coupled efficiently to all co-expressed mammalian G $\alpha_{i/o}$ -subunits
30 (G α_{i1} , G α_{i2} , G α_{i3} or G α_{o1} , and $\beta_1\gamma_2$ dimers, respectively), as was evident by the high basal
31 GTPase activities and the large absolute stimulatory and inhibitory effects of histamine and
32 thioperamide, respectively (Table 2). Also, the relative stimulatory effects of histamine and
33
34
35
36
37
38
39
40
41
42
43
44
45
46
47
48
49
50
51
52
53
54
55
56
57
58
59
60
61
62
63
64
65

1 the relative inhibitory effects of thioperamide based on total ligand-regulated GTPase activity
2 were similar for each of the four systems studied, indicating that the constitutive activity of
3 rH₃R was comparable and not substantially influenced by the type of G protein (Table 2). The
4 constitutive activity of rH₃R coupled to cognate G_i/G_o-proteins was rather high and
5 comparable to the constitutive activity of hH₃R, rendering the two systems suitable for an
6 analysis of species-specific ligand effects, without possible bias due to differences in basal
7 activity between membranes.
8
9

10 **3.4. Ligand potencies and efficacies in the steady-state GTPase assay at rH₃R** 11 **compared to hH₃R co-expressed with different G α -subunits.** 12 13

14 Next, we examined a series of imidazole-based ligands in Sf9 cell membranes expressing
15 rH₃R and different G $\alpha_{i/o}$ -proteins in the steady-state GTPase assay. The data (Table 3) were
16 then compared with the results for hH₃R [23] (Fig. 4 A and B). The endogenous agonist
17 histamine (**1**) and the standard H₃R ligands *N*^ε-methylhistamine (**2**) and (*R*)- α -
18 methylhistamine (**3**) were full agonists and equally potent in all membranes. There were
19 essentially no species-differences. The highly potent standard H₃R agonist imetit (**4**) was
20 almost a full agonist at rH₃R, too. Interestingly, proxifan (**5**) was again a strong partial agonist
21 in all systems, independent of the G protein subtype co-expressed, corroborating the notion
22 that this ligand does not show functional selectivity at H₃R_s [23]. In contrast to hH₃R,
23 impentamine (**6**) was a strong and more potent partial agonist at rH₃R in all experimental
24 settings. Strikingly, imoproxifan (**7**) was an almost full agonist at hH₃R (Fig. 5A), but an
25 inverse agonist at rH₃R (Fig. 5B). The type of G protein subunit did not change the
26 pharmacological profile of imoproxifan (Table 3). The inverse agonists ciproxifan (**8**) and
27 thioperamide (**10**) were more potent but less efficacious at rH₃R than at hH₃R and again, the
28 G protein subtype caused no changes in their profiles. Clobenpropit (**9**) was neither species-
29 specific nor did the G protein subtype change its pharmacology. Moreover, there is also a
30 strong linear correlation between potencies and efficacies of imidazole-based ligands at
31 membranes expressing rH₃R and different G $\alpha_{i/o}$ -subunits, as was found for the hH₃R (Fig. 6;
32
33
34
35
36
37
38
39
40
41
42
43
44
45
46
47
48
49
50
51
52
53
54
55
56
57
58
59
60
61
62
63
64
65

1
2
3
4
5
6
7
8
9
10
11
12
13
14
15
16
17
18
19
20
21
22
23
24
25
26
27
28
29
30
31
32
33
34
35
36
37
38
39
40
41
42
43
44
45
46
47
48
49
50
51
52
53
54
55
56
57
58
59
60
61
62
63
64
65

Table 3). Thus, the pharmacological profile of the rH₃R is also very similar under the various experimental conditions and, like at hH₃R, ligand-specific receptor conformations leading to coupling differences do not exist for the compounds investigated [23].

Collectively, these results confirm the findings regarding the relative stimulatory and inhibitory effects of histamine and thioperamide, respectively (Table 2), based on total ligand-regulated GTPase activity and are indicative for similar constitutive activity of hH₃R and rH₃R under all experimental conditions. If there had been differences in constitutive activity between hH₃R and rH₃R, then systematic changes in the potencies of full agonists as well as potencies and efficacies of partial agonists and inverse agonists would have occurred. This, however, was not the case. In contrast, the behaviour of ligands, e. g. impentamine or imoproxifan, at one H₃R species homolog often opposed each other, against every expectation. Thus, these ligand effects are solely species-specific and not due to differences in constitutive activity of hH₃R and rH₃R.

3.5. [³H]NAMH binding studies at hH₃R and rH₃R.

Since the type of G protein co-expressed did not change the pharmacology of ligands at both hH₃R and rH₃R in the steady-state GTPase assay, we performed radioligand binding experiments for a further characterization only at membranes expressing hH₃R or rH₃R plus G α_{i2} plus $\beta_1\gamma_2$ dimers.

At first, we addressed the formation of a high-affinity ternary complex between the agonist [³H]NAMH, the hH₃R or rH₃R and nucleotide-free G protein in saturation binding experiments (Fig. 5 C and D). The K_d of [³H]NAMH at hH₃R was 0.62 ± 0.21 nM, and the B_{max} was 0.62 ± 0.02 pmol/mg ($n = 3$). At rH₃R, the K_d value was 1.37 ± 0.36 nM, and the B_{max} was 0.48 ± 0.03 pmol/mg ($n = 3$). Interestingly, binding of [³H]NAMH was only slightly GTP γ S-sensitive in both cases. The K_d values of [³H]NAMH in the presence of GTP γ S (10 μ M) were about 2-fold lower, but the B_{max} values did not change significantly (Fig. 5 C and D).

1
2
3
4
5
6
7
8
9
10
11
12
13
14
15
16
17
18
19
20
21
22
23
24
25
26
27
28
29
30
31
32
33
34
35
36
37
38
39
40
41
42
43
44
45
46
47
48
49
50
51
52
53
54
55
56
57
58
59
60
61
62
63
64
65

In competition binding experiments (Fig. 4 C), histamine (1) (Fig. 5 E and F), N^α -methylhistamine (2), (*R*)- α -methylhistamine (3), imetit (4) and proxifan (5) had essentially the same affinities at hH₃R and rH₃R. Impentamine (6), imoproxifan (7) (Fig. 5 E and F), ciproxifan (8) and thioperamide (10) (Fig. 5 E and F) bound with higher affinity to rH₃R. Clobenpropit (9) also bound with similar affinity to both receptors. The pharmacological profiles, determined in [³H]NAMH competition binding (Table 4) and steady-state GTPase assays (Table 3), compared with the literature, were very similar [31, 32]. The pK_i and pEC_{50} values determined at hH₃R correlated well, suggesting a direct signal transfer in the Sf9 cell system (Fig. 7). However, at rH₃R, the correlation coefficient was rather low, due to an extraordinary high affinity of impentamine (6). Interestingly, the pK_i values of imoproxifan (7) were significantly lower than the corresponding pEC_{50} values determined in the GTPase assay (*t* test, $p < 0.05$).

3.6. Binding mode of imoproxifan at hH₃R and rH₃R.

To understand the molecular basis for the unique behaviour of imoproxifan, we performed molecular modelling studies with hH₃R and rH₃R. The binding modes of imoproxifan at active hH₃R and inactive rH₃R, representing the most favoured ligand-receptor-complexes, are presented in Fig. 8.

Imoproxifan is bound to hH₃R and rH₃R in *E*-configuration, representing the *trans*-isomer of the oxime-moiety. The *E*-configuration was also determined to be the favoured one by crystallographic studies [33]. The electrostatic surface potential of the amino acids with the ligand in the binding pocket is shown (Fig. 8, A and B). In hH₃R and rH₃R, the positively charged terminal imidazole moiety of imoproxifan interacts with the highly conserved Asp^{3.32} (Fig. 8, A and B, black arrow). However, there are large differences in electrostatic surface between TM V and TM III (Fig. 8, A and B, yellow, dotted line). In this region, the electrostatic surface potential is positive in hH₃R due to the NH moiety of Trp^{6.48}, The analogous region in rH₃R shows a slightly negative potential due to the OH moiety of Thr^{6.52}. The consequence is a different orientation, and thus a different hydrogen bond networking of the oxime moiety

1
2 of imoproxifan. In hH₃R, the methyl moiety points into direction of TM V, whereas in rH₃R, the
3 methyl moiety points downward.

4 The reason for the differences in electrostatic surface potential between hH₃R and
5 rH₃R are explained by the amino acid difference at position 3.37 between hH₃R and rH₃R. In
6 hH₃R, Glu^{5.46} can electrostatically interact with Thr^{3.37} (Fig. 8, C, yellow, dotted line). Thus,
7 Glu^{5.46} points towards Thr^{3.37} and away from the binding pocket. Consequently, the
8 electrostatic potential surface in this region is neutral and a small pocket for the methyl
9 moiety of imoproxifan is build. In contrast, in rH₃R, Thr^{3.37} is exchanged into Ala^{3.37}. Thus, an
10 electrostatic interaction between Glu^{5.46} and the amino acid side chain in position 3.37 is no
11 longer possible. Instead, the modelling studies revealed an electrostatic interaction of Glu^{5.46}
12 and Tyr^{3.33} in rH₃R (Fig. 8, D, yellow, dotted line). Consequently, the negatively charged side
13 chain of Glu^{5.46} points partially toward the binding pocket, resulting in an aromatic contact
14 between Tyr^{3.33} and the imoproxifan.
15
16
17
18
19
20
21
22
23
24
25
26
27

28 A second species-difference between hH₃R and rH₃R near to the binding pocket is
29 located at position 3.40. There is an alanine in hH₃R, but a bulkier valine in rH₃R (Fig. 8, C
30 and D, green, dotted line). It is likely that this amino acid difference also directs the oxime
31 moiety of imoproxifan into a distinct orientation. Since Ala^{3.40} is not as bulky as Val^{3.40}, there
32 is more space for the oxime moiety to point downward in direction to 3.40 in hH₃R, than in
33 rH₃R.
34
35
36
37
38
39
40
41

42 Additionally, Trp^{6.48} is shown in its active conformation at hH₃R (Fig. 8, C, blue arrow)
43 and in its inactive conformation in rH₃R (Fig. 8, D, blue arrow). Trp^{6.48} is part of a highly
44 conserved motif among GPCRs, thought to function as a toggle-switch during receptor
45 activation, as is evident due to structural and biophysical studies [34]. Trp^{6.48} horizontal to the
46 membrane surface stabilizes the active state of a GPCR. Trp^{6.48} vertical to the membrane
47 surface stabilizes the inactive state of a GPCR. As consequence of the different amino acids
48 at position 3.37 and 3.40 between hH₃R and rH₃R, the oxime moiety of imoproxifan can
49 establish a hydrogen bond interaction to Trp^{6.48} in its active conformation, thus stabilizing the
50 active conformation of hH₃R (Fig. 8, E, yellow, dotted line). This interaction was not found in
51
52
53
54
55
56
57
58
59
60
61
62
63
64
65

1
2
3
4
5
6
7
8
9
10
11
12
13
14
15
16
17
18
19
20
21
22
23
24
25
26
27
28
29
30
31
32
33
34
35
36
37
38
39
40
41
42
43
44
45
46
47
48
49
50
51
52
53
54
55
56
57
58
59
60
61
62
63
64
65

rH₃R. Here, the hydrogen of the oxime moiety interacts electrostatically with a negatively charged surface established by Thr^{6.52} (Fig. 8, F, yellow, dotted line). In rH₃R, the methyl group of imoproxifan is located in a small pocket established by Val^{3.40} and Trp^{6.48} in its inactive conformation.

Collectively, the different binding modes of imoproxifan in hH₃R and rH₃R presumably lead to differences in efficacies due to a different orientation of the oxime moiety and thus, stabilization of Trp^{6.48} either horizontal or vertical to the membrane surface.

In contrast to imoproxifan (**7**), ciproxifan (**8**) (Fig. 4B) was found to act as an inverse agonist at hH₃R as well as at rH₃R. This observation is quite interesting, since both compounds only differ in the substitution pattern at the phenyl moiety (Fig. 2). To obtain more insight into these pharmacological differences, we docked ciproxifan (**8**) into the binding pocket of the active conformation of hH₃R and performed a minimization with regard to potential energy. An overlay with the corresponding imoproxifan – hH₃R – complex showed, that the cyclopropyl moiety of ciproxifan (**8**), which is more space-filling than the methyl moiety of imoproxifan (**7**), lead to a shift of the neighbouring Glu^{5.46} away from the binding pocket. Subsequently, the hydrogen bond between Glu^{5.46} and Thr^{3.37} is broken, which may lead to a destabilization of the entire ligand-receptor complex. In contrast, ciproxifan (**8**) could be docked very well into the binding pocket of the inactive hH₃R. The resulting binding mode is similar to that of imoproxifan (**7**) at the inactive rH₃R. Since there is the smaller alanine in position 3.40 at hH₃R (compared to valine at rH₃R), the more space-filling cyclopropyl moiety fits optimally into this small pocket at hH₃R. However, the exchange of the oxime moiety into a carbonyl moiety in ciproxifan (**8**) leads to the loss of one hydrogen bond between ligand and receptor, as found for imoproxifan (Fig. 8F).

4. DISCUSSION

Ligand pharmacology at hH₃R and rH₃R is species-dependent (Fig. 4) [35, 36].

Unexpectedly, the species-differences can even span from agonism to inverse agonism in the case of imoproxifan [36]. In this study, we unraveled the underlying molecular

1
2
3
4
5
6
7
8
9
10
11
12
13
14
15
16
17
18
19
20
21
22
23
24
25
26
27
28
29
30
31
32
33
34
35
36
37
38
39
40
41
42
43
44
45
46
47
48
49
50
51
52
53
54
55
56
57
58
59
60
61
62
63
64
65

mechanism of this reversal in efficacy. In steady-state GTPase assays, imoproxifan was an inverse agonist at rH₃R, but almost full agonist at hH₃R. Competition binding studies with [³H]NAMH confirmed that the effect was receptor-mediated. Both hH₃R and rH₃R were expressed at similar levels and defined receptor-to-G protein stoichiometries. The basal activity in the two systems was comparable, as indicated by the similar inhibitory effects of the standard inverse agonist thioperamide. Thus, the unexpected behaviour of imoproxifan can only be due to species-specific differences in ligand recognition and receptor activation. Previous modelling studies described the binding mode of FUB181, a compound, similar to imoproxifan [21]. The orientation of imoproxifan in the binding pocket of H₃R, determined in the present study, is similar to these previous findings. In another study, it was suggested, that the Ala^{3.40}Val amino acid difference between hH₃R and rH₃R is responsible for the observed species-differences in antagonist pharmacology [13]. It was pointed out that thioperamide or compound A-304121 are in closer contact to Val^{3.40} in rH₃R, than to Ala^{3.40} in hH₃R. We could reproduce this finding because the affinity and potency of thioperamide was higher at rH₃R than hH₃R in our experimental system, too. Our molecular modelling studies further revealed that both amino acid differences in TM III, at position 3.37 and 3.40, are responsible for the differences in pharmacology of imoproxifan between hH₃R and rH₃R. The oxime moiety points downward in direction of Ala^{3.40} in hH₃R. Thus, the polar oxime moiety is able to establish a hydrogen bond interaction with Trp^{6.48} in its active conformation. In contrast, in rH₃R, the oxime moiety points toward TM V. Additionally, the methyl moiety of imoproxifan fits optimally into a small pocket between the bulky Val^{3.40} and Trp^{6.48} in its inactive conformation. The highly conserved Trp^{6.48} is suggested to act as a switch for receptor activation within biogenic amine receptors. Trp^{6.48} oriented horizontally to the membrane surface is thought to stabilize the active state of a receptor, while Trp^{6.48} oriented vertically to the membrane surface stabilizes the inactive state of a receptor. Since the hydrogen bond interaction between the oxime moiety and Trp^{6.48} stabilizes Trp^{6.48} in its active conformation in hH₃R, the partial agonism of imoproxifan is explained on a molecular level. This hydrogen bond-supported stabilization of Trp^{6.48} in its active conformation is not possible

1
2 in rH₃R. Here, in contrast to hH₃R, the methyl group near Val^{3.40} and Trp^{6.48} stabilizes Trp^{6.48}
3 in its inactive conformation due to a hydrophobic interaction. Thus, the modelling studies
4 provide an explanation for the inverse agonism of imoproxifan at rH₃R on a molecular level,
5
6 too. Additionally, the molecular modelling studies could be used to explain the switch from
7
8 partial agonism of imoproxifan (**7**) to inverse agonism of ciproxifan (**8**) at hH₃R. The
9
10 modelling studies suggest that the main reason for this is the more space-filling cyclopropyl
11
12 moiety of ciproxifan (**8**), compared to the methyl moiety in imoproxifan (**7**). This leads to a
13
14 loss of hydrogen bonding between Glu^{5.46} and Thr^{3.37}. Furthermore, a hydrogen bond
15
16 between the carbonyl moiety and the NH moiety of Trp^{6.48}, stabilizing the active conformation
17
18 of hH₃R, could not be established.
19
20

21
22 Interestingly, the pK_i values imoproxifan (**7**) at hH₃R and rH₃R were significantly
23
24 higher than their pEC₅₀ values (*t* test, *p* < 0.05). These results suggest that hH₃R and rH₃R
25
26 can exist in a state of low partial agonist/inverse agonist affinity that interacts efficiently with
27
28 G proteins. Another study, analyzing the hH₃R expressed in SK-N-MC cells by [³H]NAMH
29
30 competition binding and CRE-β-galactosidase reporter gene assays, revealed similar
31
32 disparities [31]. Similar results were also obtained when the human formyl peptide receptor,
33
34 coupled to various G_i-proteins, was studied in Sf9 cell membranes [37]. In this study, the K_d
35
36 of the agonist radioligand [³H]fMLP was ~100-fold lower than the EC₅₀ determined in GTPase
37
38 experiments. Interestingly, at hH₃R expressed in Sf9 cells the low affinity state stabilized by
39
40 imoproxifan (**7**) leads to an activation of G proteins, whereas in rH₃R, the low affinity state
41
42 inhibited the activation of G proteins.
43
44
45

46
47 The G protein coupling profile of hH₃R and rH₃R was similar, too (Table 2; in [23]). An
48
49 important fact is that like for hH₃R [23], at rH₃R no evidence for functional selectivity was
50
51 observed (Table 3). However, in another study, evidence for functional selectivity at H₃R
52
53 could be obtained [38]. Possible reasons for those discrepancies were already previously
54
55 discussed [23]. Both hH₃R and rH₃R coupled effectively with G_i/G_o-proteins in Sf9 cell
56
57 membranes, as was shown by GTP_γS-insensitive ternary complex formation, using
58
59 [³H]NAMH as radioligand, and steady-state [³²P]GTP hydrolysis. The similarly small shifts
60
61
62
63
64
65

1
2
3
4
5
6
7
8
9
10
11
12
13
14
15
16
17
18
19
20
21
22
23
24
25
26
27
28
29
30
31
32
33
34
35
36
37
38
39
40
41
42
43
44
45
46
47
48
49
50
51
52
53
54
55
56
57
58
59
60
61
62
63
64
65

of the [³H]NAMH saturation binding curves at hH₃R and rH₃R by GTP γ S indicate a similarly strong interaction of both receptors with the G protein and are in line with the high constitutive activity of the H₃Rs. Thus, the results confirm the data of the GTPase experiments. In line with the data for hH₃R and rH₃R, high-affinity agonist binding to the structurally closely related histamine H₄-receptor is also largely GTP γ S-insensitive [39]. The H₄-receptor possesses very high constitutive activity as well. Similar constitutive activity renders the system well suited for the analysis of species-specific ligand effects, since differences in constitutive activity between GPCRs can alter their pharmacological profiles and lead to a further complication of data interpretation [40, 41].

The pharmacology of all histamine receptors (H_xRs) is species-dependent. This is especially true for H_xR agonists. At the H₁R, several classes of bulky ligands exhibit species differences [42]. Some of them show unique behaviours, like epimeric members of the ergoline family or chiral histaprodifens, switching from silent antagonism to partial agonism depending on the species studied [28, 43]. Detailed molecular studies dissected some of the underlying mechanisms [26, 44]. At the H₂R, bulky agonists like the long-chained impromidine- and arpromidine-derived guanidines or N^G-acylated imidazolylpropylguanidines (AIPGs), are more potent and efficacious at the gpH₂R than at the hH₂R [37, 45]. Metiamide was identified to be an inverse agonist at the hH₂R, gpH₂R and rH₂R, but a weak partial agonist at the cH₂R [40]. At the H₄R, which has the lowest sequence similarity between species, studies focusing on ligand-receptor interactions of agonists are beginning to emerge [27, 46]. However, the species-differences of imoproxifan at hH₃R and rH₃R described in this study represent the most substantial differences in pharmacology among H_xRs identified so far. This is particularly compelling in view of the fact that hH₃R and rH₃R sequences display a high degree of homology and only two amino acid residues cause the disparities.

In conclusion, we have shown that hH₃R and rH₃R expressed in Sf9 cells both similarly couple to defined G_i/G_o-protein heterotrimers and display similar constitutive activities. We show species-differences in pharmacological properties of imoproxifan and offer an explanation on the molecular basis for these differences. Most importantly, we

1
2 introduce novel active state models of hH₃R and rH₃R, that are suitable to explain the
3 efficacy of H₃R ligands.
4
5
6
7

8 9 **5. ACKNOWLEDGEMENTS**

10 We would like to thank Mrs. G. Wilberg and Mrs. A. Seefeld for their excellent
11 technical assistance. Thanks are also due to the reviewers for their helpful suggestions. This
12 work was supported by the Research Training Program (Graduiertenkolleg) [GRK760]
13 “Medicinal Chemistry: Molecular Recognition – Ligand-Receptor Interactions” of the German
14 Research Foundation (DFG). The authors are affiliated with COST Action [BM0806].
15
16
17
18
19
20
21
22
23
24
25
26
27
28
29
30
31
32
33
34
35
36
37
38
39
40
41
42
43
44
45
46
47
48
49
50
51
52
53
54
55
56
57
58
59
60
61
62
63
64
65

6. REFERENCES

- 1
2 [1] Hill SJ, Ganellin CR, Timmerman H, Schwartz JC, Shankley NP, Young JM, et al.
3
4 International Union of Pharmacology. XIII. Classification of histamine receptors.
5
6 Pharmacol Rev 1997;49:253-78.
7
8
9 [2] Leurs R, Bakker RA, Timmerman H, de Esch IJ (2005) The histamine H₃ receptor: from
10
11 gene cloning to H₃ receptor drugs. Nat Rev Drug Discov 2005;4:107-20.
12
13 [3] Leurs R, Chazot PL, Shenton FC, Lim HD, de Esch IJ. Molecular and biochemical
14
15 pharmacology of the histamine H₄ receptor. Br J Pharmacol 2009;157:14-23.
16
17 [4] Zampeli E, Tiligada E. The role of histamine H₄ receptor in immune and inflammatory
18
19 disorders. Br J Pharmacol 2009;157:24-33.
20
21 [5] Tiligada E, Zampeli E, Sander K, Stark H. Histamine H₃ and H₄ receptors as novel drug
22
23 targets. Expert Opin Investig Drugs 2009;18:1519-31.
24
25 [6] Bongers G, Bakker RA, Leurs R. Molecular aspects of the histamine H₃ receptor.
26
27 Biochem Pharmacol 2007;73:1195-204.
28
29 [7] Arrang JM, Morisset S, Gbahou F. Constitutive activity of the histamine H₃ receptor.
30
31 Trends Pharmacol Sci 2007;28:350-57.
32
33 [8] Morisset S, Rouleau A, Ligneau X, Gbahou F, Tardivel-Lacombe J, Stark H, et al. High
34
35 constitutive activity of native H₃ receptors regulates histamine neurons in brain. Nature
36
37 2000;408:860-64.
38
39 [9] Ireland-Denny L, Parihar AS, Miller TR, Kang CH, Krueger KM, Esbenshade TA, et al.
40
41 Species-related pharmacological heterogeneity of histamine H₃ receptors. Eur J
42
43 Pharmacol 2001;433:141-50.
44
45 [10] Wulff BS, Hastrup S, Rimvall K. Characteristics of recombinantly expressed rat and
46
47 human histamine H₃ receptors. Eur J Pharmacol 2002;453:33-41.
48
49 [11] Ballesteros JH, Weinstein H. Integrated methods for the construction of three
50
51 dimensional models and computational probing of structure-function relations in G-protein
52
53 coupled receptors. Methods Neurosci 1995;25:366-428.
54
55
56
57
58
59
60
61
62
63
64
65

- 1
2
3
4
5
6
7
8
9
10
11
12
13
14
15
16
17
18
19
20
21
22
23
24
25
26
27
28
29
30
31
32
33
34
35
36
37
38
39
40
41
42
43
44
45
46
47
48
49
50
51
52
53
54
55
56
57
58
59
60
61
62
63
64
65
- [12] Uveges AJ, Kowal D, Zhang J, Spangler TB, Dunlop J, Semus S, et al. The role of transmembrane helix 5 in agonist binding to the human histamine H₃ receptor. *J Pharmacol Exp Ther* 2002;301:451-58.
- [13] Yao BB, Hutchins CW, Carr TL, Cassar S, Masters JN, Bennani YL, et al. Molecular modeling and pharmacological analysis of species-related histamine H₃ receptor heterogeneity. *Neuropharmacology* 2003;44:773-86.
- [14] Ligneau X, Morisset S, Tardivel-Lacombe J, Gbahou F, Ganellin CR, Stark H, et al. Distinct pharmacology of rat and human histamine H₃ receptors: role of two amino acids in the third transmembrane domain. *Br J Pharmacol* 2000;131:1247-50.
- [15] Hancock AA, Esbenshade TA, Krueger KM, Yao BB. Genetic and pharmacological aspects of histamine H₃ receptor heterogeneity. *Life Sci* 2003;73:3043-72.
- [16] Kobilka B, Schertler GF. New G-protein-coupled receptor crystal structures: insights and limitations. *Trends Pharmacol Sci* 2008;29:79-83.
- [17] Rasmussen SG, Choi HJ, Rosenbaum DM, Kobilka TS, Thian FS, Edwards PC, et al. Crystal structure of the human β_2 -adrenergic G-protein-coupled receptor. *Nature* 2007;450:383-87.
- [18] Jaakola VP, Griffith MT, Hanson MA, Cherezov V, Chien EY, Lane JR, et al. The 2.6 Å crystal structure of a human A_{2A} adenosine receptor bound to an antagonist. *Science* 2008;322:1211-17.
- [19] Park JH, Scheerer P, Hofmann KP, Choe HW, Ernst OP. Crystal structure of the ligand-free G-protein-coupled receptor opsin. *Nature* 2008;454:183-87.
- [20] Stark H, Sippl W, Ligneau X, Arrang JM, Ganellin CR, Schwartz JC, et al. Different antagonist binding properties of human and rat histamine H₃ receptors. *Bioorg Med Chem Lett* 2001;11:951-54.
- [21] Schlegel B, Laggner C, Meier R, Langer T, Schnell D, Seifert R, et al. Generation of a homology model of the human histamine H₃-receptor for ligand docking and pharmacophore-based screening. *J Comput Aided Mol Des* 2007;21:437-53.

- 1
2
3
4
5
6
7
8
9
10
11
12
13
14
15
16
17
18
19
20
21
22
23
24
25
26
27
28
29
30
31
32
33
34
35
36
37
38
39
40
41
42
43
44
45
46
47
48
49
50
51
52
53
54
55
56
57
58
59
60
61
62
63
64
65
- [22] Rai BK, Tawa GJ, Katz AH, Humblet C. Modeling G protein-coupled receptors for structure-based drug discovery using low-frequency normal modes for refinement of homology models: Application to H₃ antagonists. *Proteins* 2010;78:457-73.
- [23] Schnell D, Burleigh K, Trick J, Seifert R. No evidence for functional selectivity of proxifan at the human histamine H₃-receptor coupled to defined G_i/G_o protein heterotrimers. *J Pharmacol Exp Ther* 2010;332:996-1005.
- [24] Cherezov V, Rosenbaum DM, Hanson MA, Rasmussen SG, Thian FS, Kobilka TS, et al. High-resolution crystal structure of an engineered human β_2 -adrenergic G protein-coupled receptor. *Science* 2007;318:1258-65.
- [25] Strasser A, Wittmann HJ. Analysis of the activation mechanism of the guinea-pig Histamine H₁-receptor. *J Comput Aided Mol Des* 2007;21:499-509.
- [26] Strasser A, Wittmann HJ, Seifert R. Ligand-specific contribution of the N terminus and E2-loop to pharmacological properties of the histamine H₁-receptor. *J Pharmacol Exp Ther* 2008;326:783-91.
- [27] Igel P, Geyer R, Strasser A, Dove S, Seifert R, Buschauer A. Synthesis and structure-activity relationships of cyanoguanidine-type and structurally related histamine H₄ receptor agonists. *J Med Chem* 2009;52:6297-6313.
- [28] Strasser A, Striegl B, Wittmann HJ, Seifert R. Pharmacological profile of histaprodifens at four recombinant histamine H₁-receptor species isoforms. *J Pharmacol Exp Ther* 2008;324:60-71.
- [29] van der Spoel D, Lindahl E, Hess B, Groenhof G, Mark AE, Berendsen HJC. GROMACS: fast, flexible, and free. *J Comput Chem* 2005;26:1701-18.
- [30] Thompson JD, Higgins DG, Gibson TJ. CLUSTAL W: improving the sensitivity of progressive multiple sequence alignment through sequence weighting, position-specific gap penalties and weight matrix choice. *Nucleic Acids Res* 1994;22:4673-80
- [31] Lim HD, van Rijn RM, Ling P, Bakker RA, Thurmond RL, Leurs R. Evaluation of histamine H₁-, H₂-, and H₃-receptor ligands at the human histamine H₄ receptor:

- 1 identification of 4-methylhistamine as the first potent and selective H₄ receptor agonist. J
2 Pharmacol Exp Ther 2005;314:1310-21.
3
- 4 [32] Bongers G, Krueger KM, Miller TR, Baranowski JL, Estvander BR, Witte DG, et al. An
5
6 80-amino acid deletion in the third intracellular loop of a naturally occurring human
7
8 histamine H₃ isoform confers pharmacological differences and constitutive activity. J
9
10 Pharmacol Exp Ther 2007;323:888-98.
11
- 12 [33] Sasse A, Sadek B, Ligneau X, Elz S, Pertz HH, Luger P, et al. New histamine H₃-
13
14 receptor ligands of the proxifan series: imoproxifan and other selective antagonists with
15
16 high oral *in vivo* potency. J Med Chem 2000;43:3335-43.
17
18
- 19 [34] Ahuja S and Smith SO. Multiple switches in G protein-coupled receptor activation.
20
21 Trends Pharmacol Sci 2009;30:494-502.
22
- 23 [35] Lovenberg TW, Pyati J, Chang H, Wilson SJ, Erlander MG. Cloning of rat histamine H₃
24
25 receptor reveals distinct species pharmacological profiles. J Pharmacol Exp Ther
26
27 2000;293:771-778.
28
29
- 30 [36] Esbenshade TA, Estvander BR, Miller TR, Baranowski JL, Sharma R, Hancock AA,
31
32 Krueger KM. Pharmacological classification of histamine H₃ receptor agents across
33
34 species is attributable to transmembrane 3 sequence differences. Inflamm Res 2007;56
35
36 Suppl 1:S45-S46.
37
38
- 39 [37] Wenzel-Seifert K, Arthur JM, Liu HY, Seifert R. Quantitative analysis of formyl peptide
40
41 receptor coupling to G α_{11} , G α_{12} , and G α_{13} . J Biol Chem 1999;274:33259-66.
42
43
- 44 [38] Krueger KM, Witte DG, Ireland-Denny L, Miller TR, Baranowski JL, Buckner S, Milicic I,
45
46 Esbenshade TA, Hancock AA. G protein-dependent pharmacology of histamine H₃
47
48 receptor ligands: evidence for heterogeneous active state receptor conformations. J
49
50 Pharmacol Exp Ther 2005;314:271-278.
51
- 52 [39] Schneider EH, Schnell D, Papa D, Seifert R. High constitutive activity and a G-protein-
53
54 independent high-affinity state of the human histamine H₄-receptor. Biochemistry
55
56 2009;48:1424-1438.
57
58
59
60
61
62
63
64
65

- 1
2
3
4
5
6
7
8
9
10
11
12
13
14
15
16
17
18
19
20
21
22
23
24
25
26
27
28
29
30
31
32
33
34
35
36
37
38
39
40
41
42
43
44
45
46
47
48
49
50
51
52
53
54
55
56
57
58
59
60
61
62
63
64
65
- [40] Preuss H, Ghorai P, Kraus A, Dove S, Buschauer A, Seifert R. Constitutive activity and ligand selectivity of human, guinea pig, rat, and canine histamine H₂ receptors. *J Pharmacol Exp Ther* 2007;321:983-95.
- [41] Preuss H, Ghorai P, Kraus A, Dove S, Buschauer A, Seifert R. Mutations of Cys-17 and Ala-271 in the human histamine H₂ receptor determine the species selectivity of guanidine-type agonists and increase constitutive activity. *J Pharmacol Exp Ther* 2007;321:975-82.
- [42] Seifert R, Wenzel-Seifert K, Bürckstümmer T, Pertz HH, Schunack W, Dove S, et al. Multiple differences in agonist and antagonist pharmacology between human and guinea pig histamine H₁-receptor. *J Pharmacol Exp Ther* 2003;305:1104-15.
- [43] Pertz HH, Gornemann T, Schurad B, Seifert R, Strasser A. Striking differences of action of lisuride stereoisomers at histamine H₁ receptors. *Naunyn Schmiedebergs Arch Pharmacol* 2006;374:215-22.
- [44] Strasser A, Wittmann HJ, Kunze M, Elz S, Seifert R. Molecular basis for the selective interaction of synthetic agonists with the human histamine H₁-receptor compared with the guinea pig H₁-receptor. *Mol Pharmacol* 2009;75:454-465.
- [45] Kelley MT, Bürckstümmer T, Wenzel-Seifert K, Dove S, Buschauer A, Seifert R. Distinct interaction of human and guinea pig histamine H₂-receptor with guanidine-type agonists. *Mol Pharmacol* 2001;60:1210-1225.
- [46] Lim HD, Jongejan A, Bakker RA, Haaksma E, de Esch IJ, Leurs R. Phenylalanine 169 in the second extracellular loop of the human histamine H₄ receptor is responsible for the difference in agonist binding between human and mouse H₄ receptors. *J Pharmacol Exp Ther* 2008;327:88-96.

FIGURE CAPTIONS

1
2
3
4
5
6
7
8
9
10
11
12
13
14
15
16
17
18
19
20
21
22
23
24
25
26
27
28
29
30
31
32

Fig. 1. Comparison of the amino acid sequences of hH₃R (GeneBank Accession No. AF140538) and rH₃R (GeneBank Accession No. AF237919). Putative transmembrane domains are stated above the sequences and indicated by a solid line. N-term, extracellular N-terminal domain of H₃Rs; C-term, intracellular C-terminal domain of H₃Rs; i1, i2, and i3, first, second, and third intracellular loops; e1, e2, e3, first, second, and third extracellular loops, respectively. Dots in the sequence of rH₃R indicate identity with hH₃R. Amino acids shown in regular fonts in the sequence of rH₃R represent conservative differences, those shown in bold represent non-conservative differences. The most conserved residues in each TM domain are indicated in grey shading. Residues within TM domains are named according to the Ballesteros/Weinstein nomenclature. The most conserved residue in each TM is numbered as X.50, where X is the number of the respective TM domain [11]. Amino acids shown in white with black shading represent a putative glycosylation site of the H₃R. Amino acids in frame represent putative interaction sites of HA with the H₃R [12, 13].

33
34
35
36
37
38
39

Fig. 2. Structures of imidazole-containing H₃R-ligands: full agonists **1-3**, partial agonists **4-6**, imoproxifan **7**, and antagonists/inverse agonists **8-10**.

40
41
42
43
44
45
46
47
48
49
50
51
52
53
54
55
56
57
58
59
60
61
62
63
64
65

Fig. 3. Immunological detection of hH₃R and rH₃R expressed in Sf9 cells. Each lane of the gels was loaded with 10 µg of membrane protein, unless otherwise indicated below the film. Numbers on the left designate masses of marker proteins in kDa. In **A** and **B**, membranes expressing the hH₃R and rH₃R alone were loaded onto the gels. Proteins separated in **A** were reacted with anti-hH₃R Ig and in **B** with anti-rH₃R Ig. In **C**, membranes of **A** and **B** plus control were analyzed. Here, the proteins were reacted with the non-species-selective anti-hH₃R (i3) Ig. In **D1** and **D2**, 2, 4, 6, 8 and 10 µg of protein of Sf9 membranes expressing hβ₂AR at 7.5 pmol/mg (as determined by [³H]dihydroalprenolol saturation binding) were used as standard to assess the expression levels of the rH₃R in different membrane preparations with anti-FLAG Ig. In **E**, the same membranes were reacted with anti-His6 Ig. In

1
2
3
4
5
6
7
8
9
10
11
12
13
14
15
16
17
18
19
20
21
22
23
24
25
26
27
28
29
30

F, the membranes were reacted with anti-G $\alpha_{i\text{-common}}$ Ig. In **G**, the membranes were reacted with anti-G $\beta\text{-common}$ Ig. In **H**, 0.5, 1.0, 1.5 and 2.0 μg of a membrane expressing the rH $_3$ R + G α_{i2} + $\beta_1\gamma_2$ was analyzed in order to quantify the G α -subunits, using 2, 4, 7.5, 15 and 30 pmol of purified G α_{i2} as standard. In **I**, 0.5, 1.0, 1.5 and 2.0 μg of a corresponding membrane of the same batch expressing rH $_3$ R + G α_{o1} + $\beta_1\gamma_2$ was analyzed to quantify the G α -subunits, using 2, 4, 7.5, 15 and 30 pmol of purified G α_{o2} an almost identical splice variant of G α_{o1} as standard.

31
32
33
34
35
36
37
38
39
40
41
42
43
44
45
46
47
48
49
50
51
52
53
54
55
56
57
58
59
60
61
62
63
64
65

Fig. 4. Comparison of the pharmacological properties of hH $_3$ R and rH $_3$ R. **A**, Comparison of the potencies of ligands in the GTPase assay. Data for hH $_3$ R were taken from Ref. 23, data for rH $_3$ R were taken from Table 3. **B**, Comparison of the efficacies of ligands in the GTPase assay. Data for hH $_3$ R were taken from Ref. 23, data for rH $_3$ R were taken from Table 3. **C**, Comparison of the affinities of ligands in the [^3H]NAMH competition binding assay. Data were taken from Table 4.

Fig. 5. Comparison of the effects of histamine, imoproxifan and thioperamide in membranes co-expressing the hH $_3$ R or rH $_3$ R, G α_{i2} subunits and $\beta_1\gamma_2$ dimers. **A** and **B**, Steady-state GTPase activity in Sf9 membranes was determined as described under *Methods*. Reaction mixtures contained HA, IMO or THIO at the concentrations indicated on the abscissa to achieve saturation. Data are expressed as percentage change in GTPase activity induced by the ligands compared to the GTPase activity stimulated by HA (10 μM), which was defined to be 100%. Data were analyzed by nonlinear regression and were best fit to sigmoidal concentration/response curves. Data points shown are the means \pm S. E. M. of 3 - 4 independent experiments performed in duplicate. A summary of all results is shown in Table 3. **C** and **D**, [^3H]NAMH saturation binding experiments were performed as described under *Methods*. Data were analyzed by nonlinear regression and were best fitted to hyperbolic one-site saturation isotherms. The closed circles (\bullet) show the data for the specific [^3H]NAMH binding in the absence of GTP γS (10 μM), the open circles (\circ) in the presence of GTP γS (10 μM). In **C**, hH $_3$ R was analyzed and in **D**, rH $_3$ R was analyzed. Data points shown

are the means \pm S. E. M. of 3 independent experiments performed in triplicate, using three different membrane preparations. **E** and **F**, [3 H]NAMH binding was determined as described under *Methods*. Reaction mixtures contained Sf9 membranes (10 - 50 μ g of protein per tube) expressing the recombinant proteins, 1 nM [3 H]NAMH, and ligands at the concentrations indicated on the abscissa. **E**, competition binding at hH₃R and **F**, competition binding at rH₃R. Data were analyzed for best fit to monophasic competition curves (*F* test). Data points shown are the means \pm S. E. M. of 3 - 5 independent experiments performed in duplicate.

Fig. 6. Correlation of potency and efficacy of ligands at the rH₃R in the presence of different co-expressed G $\alpha_{i/o}$ -proteins. Data shown in Table 3 were analyzed by linear regression. Numbers designate individual ligands decoded in Fig. 2. In **A**, **C** and **E**, the potencies of ligands at membranes co-expressing the rH₃R, G α_{i1} , G α_{i3} or G α_{o1} , and $\beta_1\gamma_2$ -dimers, respectively, were correlated with values determined at the reference membrane expressing G α_{i2} . **A**, $r^2 = 0.77$; $slope = 0.99 \pm 0.19$. **C**, $r^2 = 0.97$; $slope = 1.17 \pm 0.07$. **E**, $r^2 = 0.96$; $slope = 1.05 \pm 0.07$. In **B**, **D** and **F**, the efficacies of ligands at membranes co-expressing the rH₃R, G α_{i1} , G α_{i3} or G α_{o1} , and $\beta_1\gamma_2$ dimers, respectively, were correlated with values determined at the reference membrane expressing G α_{i2} . **B**, $r^2 = 0.99$; $slope = 0.97 \pm 0.04$. **D**, $r^2 = 0.96$; $slope = 0.99 \pm 0.07$. **F**, $r^2 = 0.996$; $slope = 1.20 \pm 0.03$. The dotted lines indicate the 95% confidence intervals of the regression lines. The diagonal dashed line has a slope of 1 and represents a theoretical curve for identical values.

Fig. 7. Correlation of affinity and potency of ligands at the hH₃R and rH₃R. Data shown were analyzed by linear regression. Numbers designate individual ligands decoded in Fig. 2. In **A**, the affinities and potencies of ligands at membranes co-expressing the hH₃R, G α_{i2} and $\beta_1\gamma_2$ dimers were correlated. **A**, $r^2 = 0.83$; $slope = 0.94 \pm 0.15$. In **B**, the affinities and potencies of ligands at membranes co-expressing the rH₃R, G α_{i2} and $\beta_1\gamma_2$ dimers were correlated. **B**, $r^2 = 0.50$; $slope = 0.83 \pm 0.29$. The dotted lines indicate the 95% confidence

intervals of the regression lines. The diagonal dashed line has a slope of 1 and represents a theoretical curve for identical values.

Fig. 8. Binding mode of imoproxifan at the active hH₃R and inactive rH₃R.

A, electrostatic potential surface in the binding pocket of active hH₃R with imoproxifan in its binding conformation. **B**, electrostatic potential surface in the binding pocket of the inactive rH₃R with imoproxifan in its binding conformation. **A** and **B**, yellow dotted circle: the electrostatic potential is rather positive at hH₃R due to the NH moiety of Trp^{6.48}, but slightly negatively charged in rH₃R due to the OH moiety of Thr^{6.52}. The consequence is a different orientation of the ligands oxime moiety. **C**, conformation of amino acids in the imoproxifan bound state of active hH₃R. **D**, conformation of amino acids in the imoproxifan bound state of inactive rH₃R. **C** and **D**, yellow dotted circle: important differences in side chain conformation of Glu^{5.46} between hH₃R and rH₃R. At hH₃R, Glu^{5.46} interacts with Thr^{3.37} and points away from the binding pocket. In rH₃R, Thr^{3.37} is exchanged to Ala^{3.37}. Thus, the interaction between Glu^{5.46} and the amino acid in position 3.37 is no longer possible and Glu^{5.46} interacts with Tyr^{3.33}. Green dotted circle: in position 3.40, there is a small Ala in hH₃R, but the more bulky Val at rH₃R. It is suggested that this species difference is also be important for the different orientations of the oxime moiety between hH₃R and rH₃R. **E**, interaction between imoproxifan and hH₃R; **F**, interaction between imoproxifan and rH₃R. **E** and **F**, yellow dotted circle: at hH₃R, the oxime moiety of imoproxifan points downwards and stabilizes the highly conserved Trp^{6.48} in its active conformation by a hydrogen bond; at rH₃R, the oxime moiety of imoproxifan points upwards to TM V and interacts with Thr^{6.52}.

TABLES

Table 1: Quantification of rH₃R-to-G protein ratios via western blot, [³H]JNJ-7753707- and [³⁵S]GTP_γS-saturation binding.

membrane	$B_{\max} \pm S. E. M. (\text{pmol} \times \text{mg}^{-1})$			
	rH ₃ R + $\beta_1\gamma_2$			
	+ G α_{i1}	+ G α_{i2}	+ G α_{i3}	+ G α_{o1}
immunoblot: anti-FLAG Ig	~1.5 – 2.5	~1.5 – 2.5	~1.5 – 2.5	~1.5 – 2.5
anti-G α Igs	n. d.	~50 - 100	n. d.	~50 - 100
[³ H]JNJ-7753707	0.67 ± 0.03	0.77 ± 0.02	1.05 ± 0.04	1.25 ± 0.04
[³⁵ S]GTP _γ S	3.40 ± 0.80	4.43 ± 0.53	2.52 ± 0.37	8.19 ± 1.27
R : G ratio	~1 : 5	~1 : 6	~1 : 2	~1 : 7

The quantification of receptors and G proteins via immunoblot was performed as described [23]. [³H]JNJ-7753707 saturation bindings were performed as described under *Methods*. [³⁵S]GTP_γS saturation bindings were performed, using Sf9 cell membranes from the same batch of preparation. Reaction mixtures contained membranes (10 - 20 μg of protein), 0.2 - 2 nM of [³⁵S]GTP_γS, and unlabeled GTP_γS to give the desired final ligand concentrations for saturation (0.2 – 50 nM). GDP or additional H₃R ligands were not present in the reaction mixtures. Data were analyzed by nonlinear regression and were best fitted to hyperbolic one-site saturation isotherms. The maximal number of GTP_γS binding sites in membranes expressing rH₃R plus G α_{i2} plus $\beta_1\gamma_2$ was corrected by the binding determined in rH₃R plus $\beta_1\gamma_2$. By this way, the number of functionally intact and heterologously expressed G protein α -subunits was quantified. Data shown are the means ± S. E. M. of 3 independent experiments performed in triplicate. Receptor-to-G protein ratios were calculated, using the B_{\max} values determined for the different membrane preparations.

Table 2: Analysis of rH₃R/G protein coupling - GTPase activities in Sf9 membranes expressing rH₃R and different G $\alpha_{i/o}$ -proteins.

GTPase activity ± S. E. M.	rH ₃ R + $\beta_1\gamma_2$			
	+ G α_{i1}	+ G α_{i2}	+ G α_{i3}	+ G α_{o1}
basal (pmol × mg ⁻¹ × min ⁻¹)	1.22 ± 0.21	1.75 ± 0.22	1.12 ± 0.04	4.29 ± 0.12
+ ago. (pmol × mg ⁻¹ × min ⁻¹)	2.01 ± 0.26	3.17 ± 0.37	2.13 ± 0.14	5.95 ± 0.14
Δ ago. (pmol × mg ⁻¹ × min ⁻¹)	0.79 ± 0.07	1.42 ± 0.15	1.01 ± 0.10	1.66 ± 0.09
Agonist stimulation (% of basal)	67.44 ± 0.09	81.78 ± 2.32	89.38 ± 5.14	38.78 ± 2.38
+ inv. ago. (pmol × mg ⁻¹ × min ⁻¹)	0.71 ± 0.10	0.85 ± 0.12	0.59 ± 0.03	2.86 ± 0.14
Δ inv. ago. (pmol × mg ⁻¹ × min ⁻¹)	0.51 ± 0.13	0.90 ± 0.10	0.53 ± 0.02	1.43 ± 0.13
Inverse agonist inhibition (% of basal)	40.32 ± 5.93	51.66 ± 0.96	47.4 ± 0.82	33.29 ± 2.88

Steady-state GTPase experiments were performed as described in *Methods*. Reaction mixtures contained 0.1 μ Ci [γ -³²P]GTP and 100 nM unlabeled GTP in the presence of solvent (basal), 10 μ M HA (+ ago.) or 10 μ M THIO (+ inv. ago.). Data shown are the means ± S. E. M. of three to four independent experiments for each membrane preparation performed in duplicates. The absolute agonist-stimulation (Δ ago.) and inverse agonist-inhibition (Δ inv. ago.) of GTP hydrolysis, as well as the relative agonist-stimulation and inverse agonist-inhibition of GTP hydrolysis (% of basal), were calculated.

Table 3: Ligand potencies and efficacies in the GTPase assay at Sf9 cell membranes expressing the rH₃R and different G proteins.

	rH ₃ R + G α_{i1} + $\beta_1\gamma_2$		rH ₃ R + G α_{i2} + $\beta_1\gamma_2$		rH ₃ R + G α_{i3} + $\beta_1\gamma_2$		rH ₃ R + G α_{o1} + $\beta_1\gamma_2$	
	pEC ₅₀	E _{max} ± S. E. M.	pEC ₅₀	E _{max} ± S. E. M.	pEC ₅₀	E _{max} ± S. E. M.	pEC ₅₀	E _{max} ± S. E. M.
	± S. E. M.		± S. E. M.		± S. E. M.		± S. E. M.	
HA	7.64 ± 0.07*	1.00	7.94 ± 0.05	1.00	7.88 ± 0.06	1.00	7.72 ± 0.05	1.00
NAMH	8.30 ± 0.23	0.91 ± 0.10	8.98 ± 0.12	1.06 ± 0.07	9.11 ± 0.30	1.16 ± 0.21	8.88 ± 0.18	1.10 ± 0.11
RAMH	8.06 ± 0.17	0.88 ± 7.14	8.54 ± 0.10	0.91 ± 0.05	8.50 ± 0.08	0.90 ± 0.03	8.21 ± 0.10	0.84 ± 0.04
IME	9.86 ± 0.19	0.95 ± 0.10	9.76 ± 0.13	0.89 ± 0.06	10.14 ± 0.36	1.39 ± 0.30	9.78 ± 0.12	0.99 ± 0.07
PRO	8.12 ± 0.22	0.48 ± 0.05	8.52 ± 0.12	0.66 ± 0.04	8.42 ± 0.10	0.64 ± 0.04	8.19 ± 0.16	0.66 ± 0.05
IMP	8.33 ± 0.15	0.72 ± 0.05	8.94 ± 0.20	0.91 ± 0.10	8.99 ± 0.26	0.95 ± 0.14	8.76 ± 0.12	0.84 ± 0.06
IMO	9.03 ± 0.26	-0.61 ± 0.08	9.03 ± 0.13	-0.61 ± 0.04	9.05 ± 0.23	-0.46 ± 0.05	8.93 ± 0.16	-0.96 ± 0.08**
CIP	8.71 ± 0.27	-0.81 ± 0.10	8.64 ± 0.10	-0.75 ± 0.03	8.64 ± 0.15	-0.61 ± 0.04	8.58 ± 0.16	-1.01 ± 0.07
CLOB	9.04 ± 0.26	-0.43 ± 0.05	8.95 ± 0.16	-0.44 ± 0.03	8.77 ± 0.13	-0.41 ± 0.02	8.68 ± 0.11	-0.69 ± 0.03**
THIO	7.82 ± 0.24	-0.66 ± 0.07	7.66 ± 0.12	-0.62 ± 0.03	7.61 ± 0.13	-0.50 ± 0.03	7.64 ± 0.08	-0.99 ± 0.03***
<i>r</i> ²	0.77	0.99	1.00	1.00	0.97	0.96	0.96	0.996
<i>slope</i>	0.99 ± 0.19	0.97 ± 0.04	1.00	1.00	1.17 ± 0.07	0.99 ± 0.07	1.05 ± 0.07	1.20 ± 0.03

1
2
3
4
5
6 Steady-state GTPase activity in Sf9 membranes expressing rH₃R, different G $\alpha_{i/o}$ subunits and $\beta_1\gamma_2$ was determined as described under *Materials*
7 *and Methods*. Reaction mixtures contained ligands at concentrations from 0.1 nM to 10 μ M as appropriate to generate saturated
8 concentration/response curves. Data were analyzed by nonlinear regression and were best fit to sigmoid concentration/response curves. Typical
9 basal GTPase activities ranged between 1.0 and 4.0 pmol * mg⁻¹ * min⁻¹, and the maximal stimulatory effect of histamine (10 μ M) amounted to ~40
10 to ~90% above basal. The efficacy (E_{max}) of histamine was determined by nonlinear regression and was set to 1.00. The E_{max} values of other
11 agonists and inverse agonists were referred to this value. Data shown are the means \pm S. E. M. of three to four experiments performed in
12 duplicates each. Statistical analysis was performed using one-way ANOVA, followed by Dunnet's multiple comparison test using the values
13 determined at hH₃R, G α_{i2} and $\beta_1\gamma_2$ as a reference. Significant differences to the membrane expressing G α_{i2} are shown following comparison with
14 other G $\alpha_{i/o}$ subunits. (no symbol: not significant; *, $p < 0.05$; **, $p < 0.01$; ***, $p < 0.001$). Additionally, data shown were correlated and analyzed by
15 linear regression. The potencies and efficacies of ligands at membranes co-expressing the rH₃R, G α_{i1} , G α_{i3} or G α_{o1} , and $\beta_1\gamma_2$ dimers, respectively,
16 were correlated with values determined at the reference membrane expressing G α_{i2} . The correlation coefficients (r^2) and the *slopes* are presented
17 at the bottom of the table.
18
19
20
21
22
23
24
25
26
27
28
29
30
31
32
33
34
35
36
37
38
39
40
41
42
43
44
45
46
47
48
49

Table 4: [³H]NAMH competition bindings in Sf9 membranes expressing hH₃R or rH₃R in combination with G_{α_{i2}} and β₁γ₂.

	pK _i ± S. E. M.	
	hH ₃ R + G _{α_{i2}} + β ₁ γ ₂	rH ₃ R + G _{α_{i2}} + β ₁ γ ₂
HA	8.20 ± 0.04	7.89 ± 0.07
NAMH	9.22 ± 0.03	8.70 ± 0.09
RAMH	8.91 ± 0.07	8.62 ± 0.07
IME	9.20 ± 0.05	9.38 ± 0.08
PRO	7.87 ± 0.07	8.08 ± 0.10
IMP	8.84 ± 0.06	10.11 ± 0.05
IMO	6.92 ± 0.06	8.47 ± 0.09
CIP	7.03 ± 0.12	8.87 ± 0.08
CLOB	9.34 ± 0.06	9.11 ± 0.06
THIO	7.34 ± 0.04	7.94 ± 0.04
<i>r</i> ² (pK _i /pEC ₅₀)	0.83	0.50
<i>slope</i> (pK _i /pEC ₅₀)	0.94 ± 0.15	0.83 ± 0.29

Experiments were performed as described under *Methods*. Reaction mixtures contained Sf9 membranes (10 – 50 μg of protein), 1 nM [³H]NAMH, and unlabeled ligands at concentrations of 0.1 nM to 10 μM as appropriate to generate saturated competition curves. Data were analyzed by nonlinear regression and were best fit to one-site (monophasic) competition curves. Data shown are the means ± S. E. M. of three to five independent experiments performed in duplicate at 3 different membrane preparations. Additionally, data shown were correlated and analyzed by linear regression. The affinities and potencies of ligands at membranes co-expressing the hH₃R or rH₃R plus G_{α_{i2}} plus β₁γ₂ dimers, respectively, were correlated. The correlation coefficients (*r*²) and the *slopes* of all tested ligands are presented at the bottom of the table.

Fig. 1

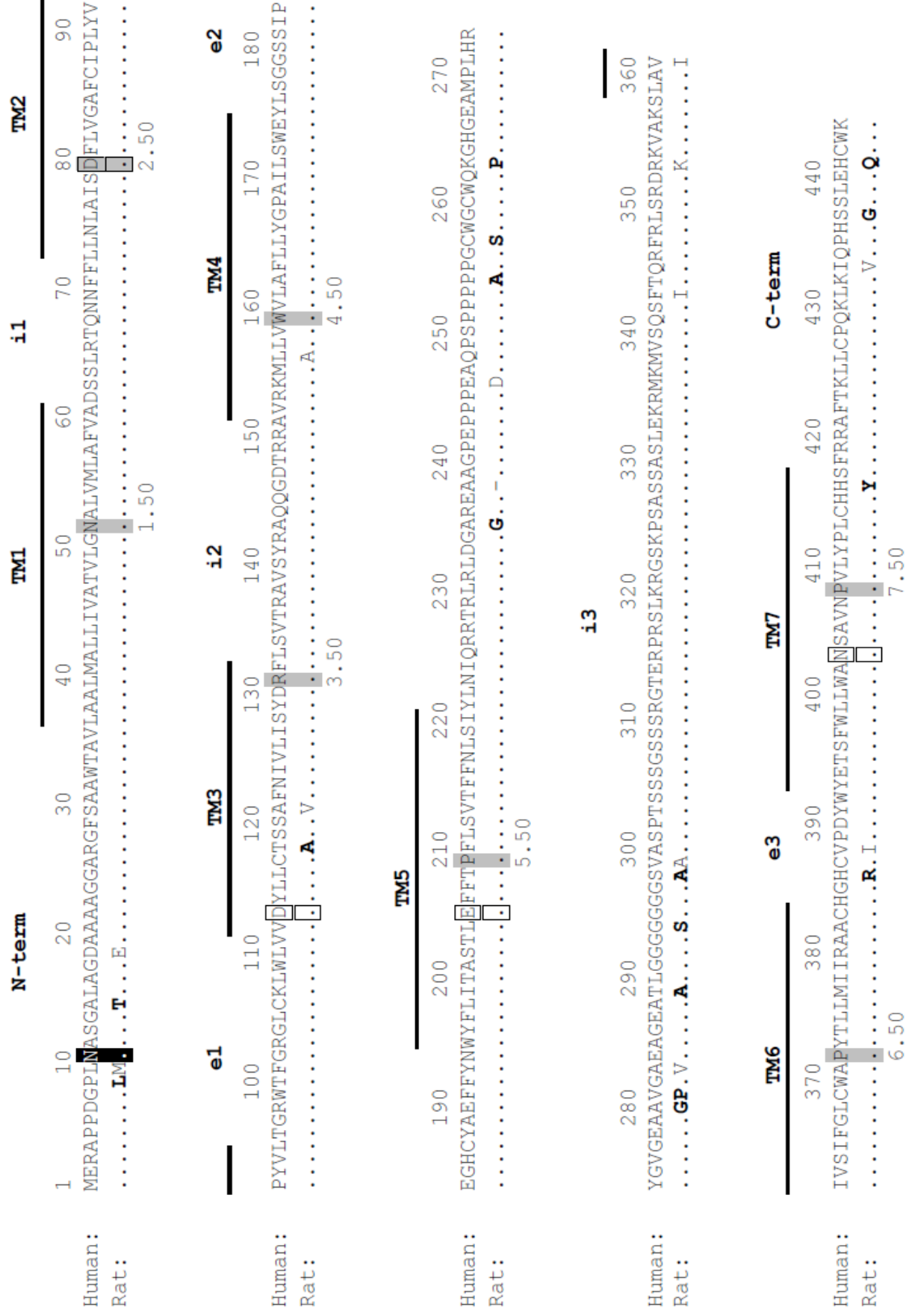


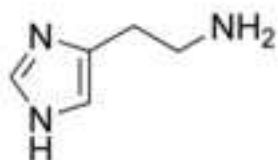
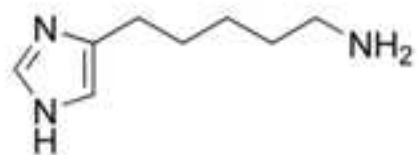
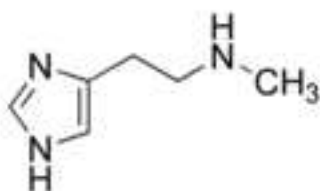
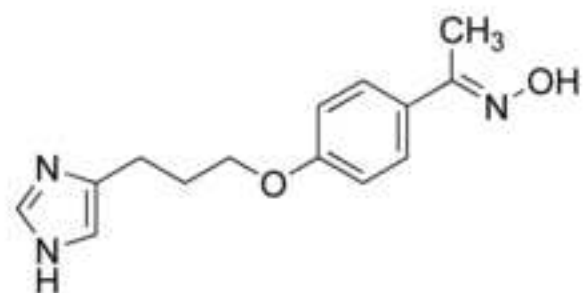
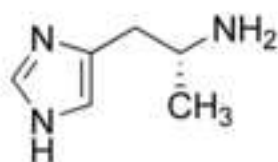
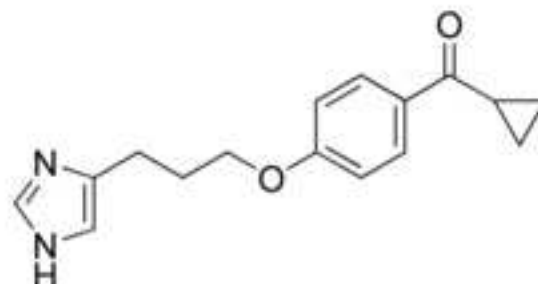
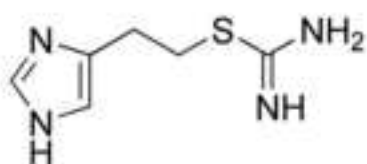
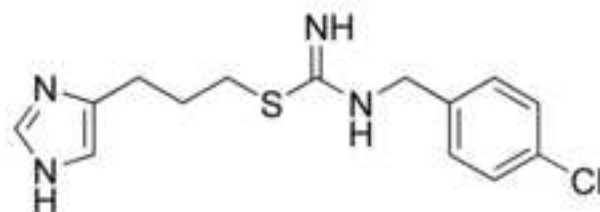
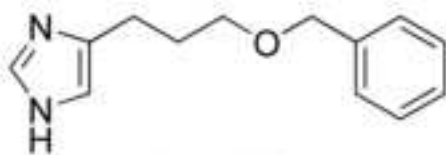
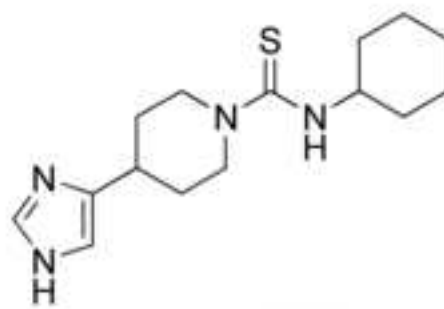
Fig. 2histamine (HA), **1**impentamine (IMP), **6** N^{α} -methylhistamine
(NAMH), **2**imoproxifan (IMO), **7**(R)- α -methylhistamine
(RAMH), **3**ciproxifan (CIP), **8**imetit (IME), **4**clobenpropit (CLOB), **9**proxifan (PRO), **5**thioperamide (THIO), **10**

Figure 3

Fig. 3

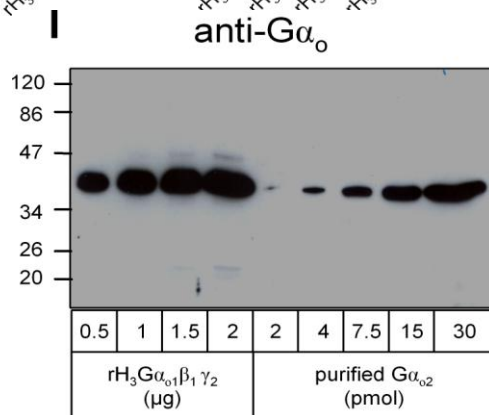
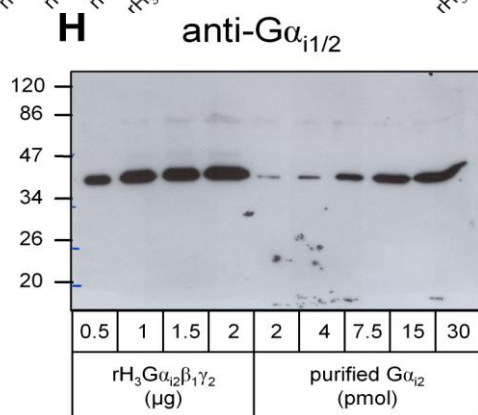
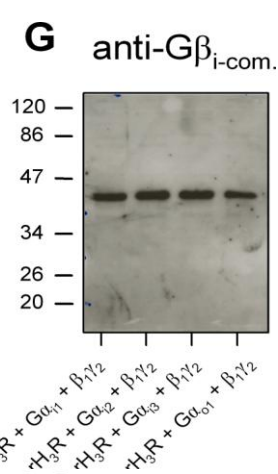
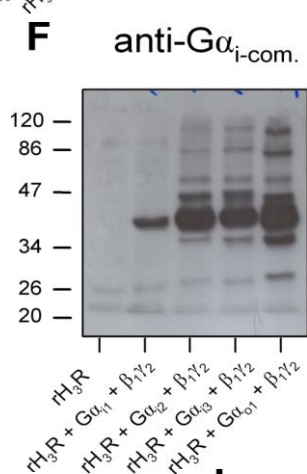
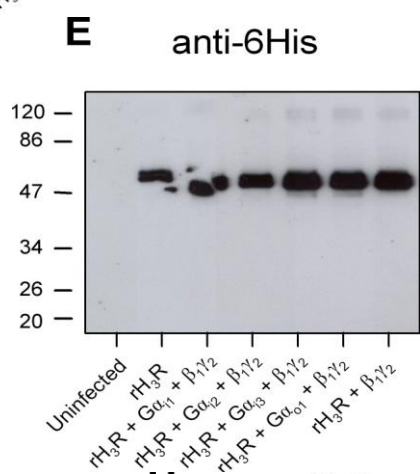
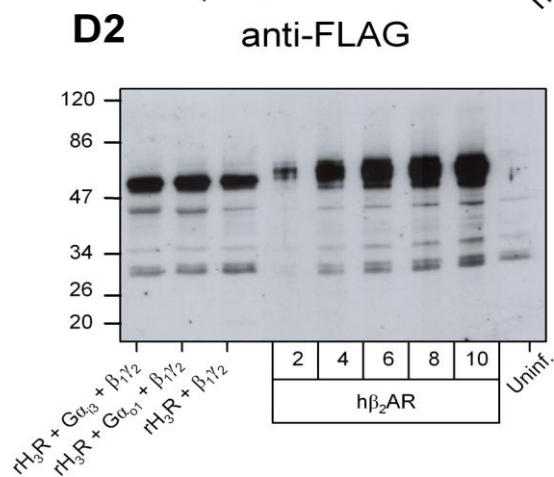
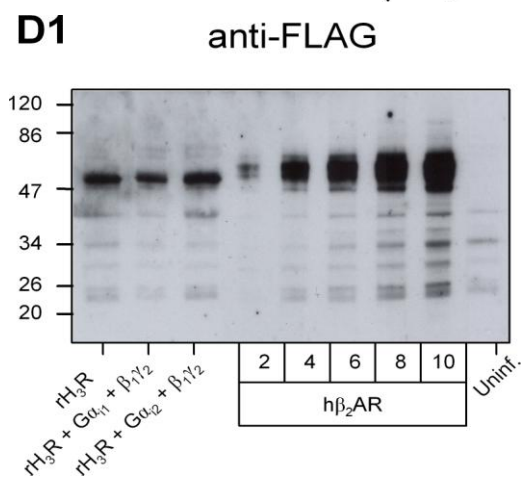
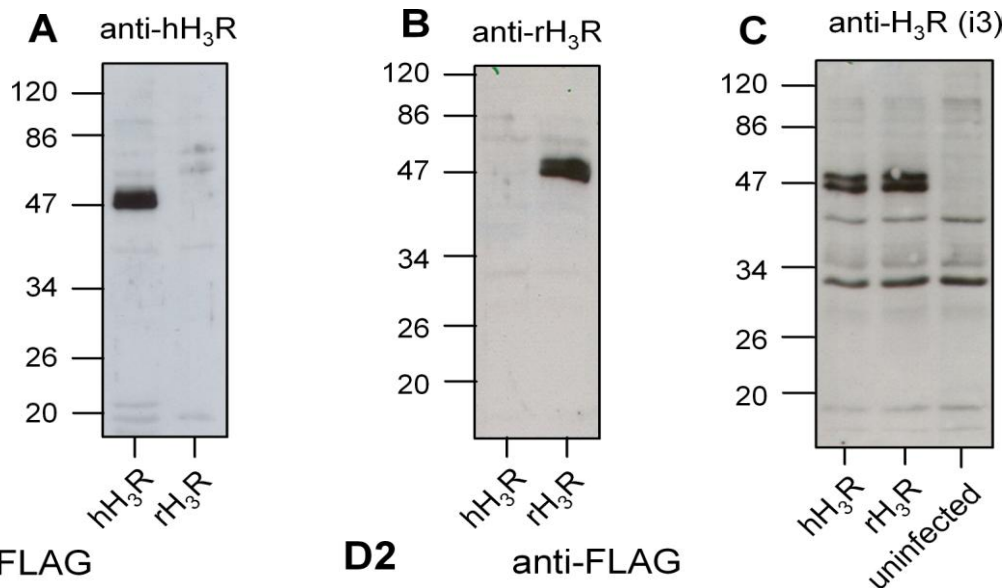


Figure 4

Fig. 4

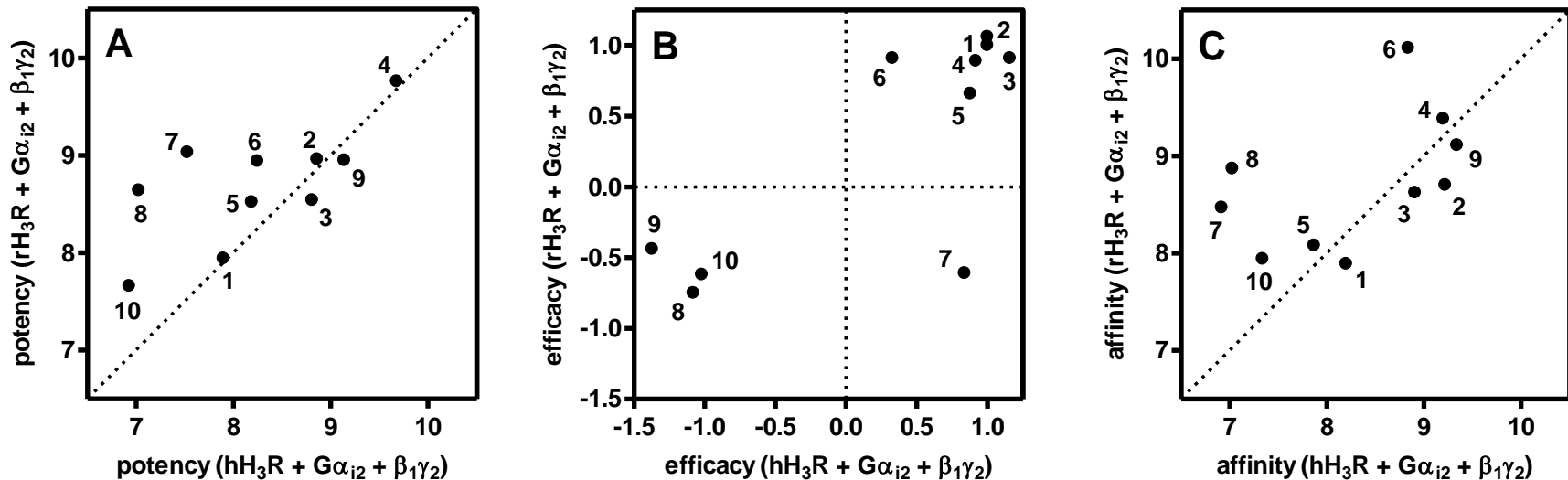


Fig. 5

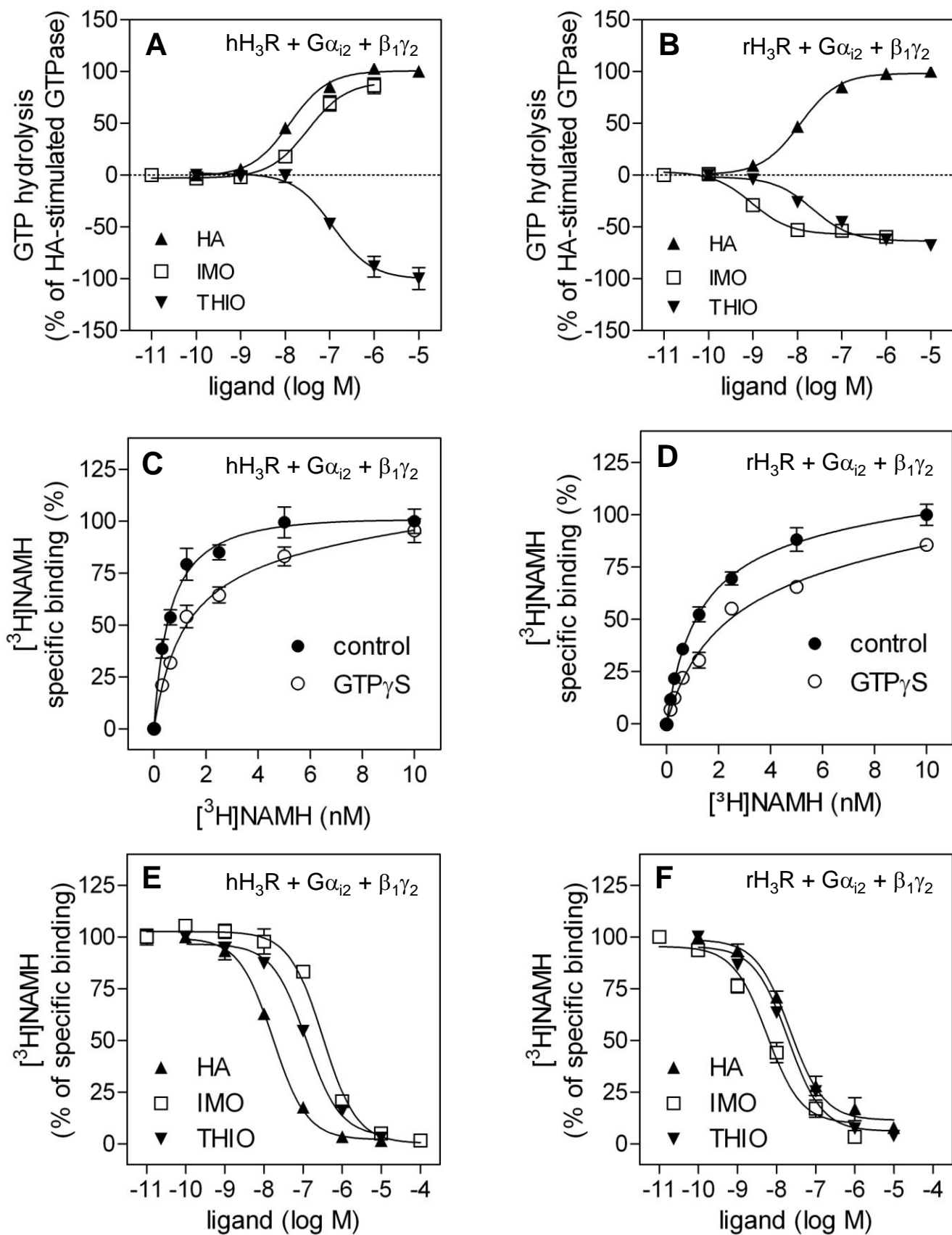


Fig. 6

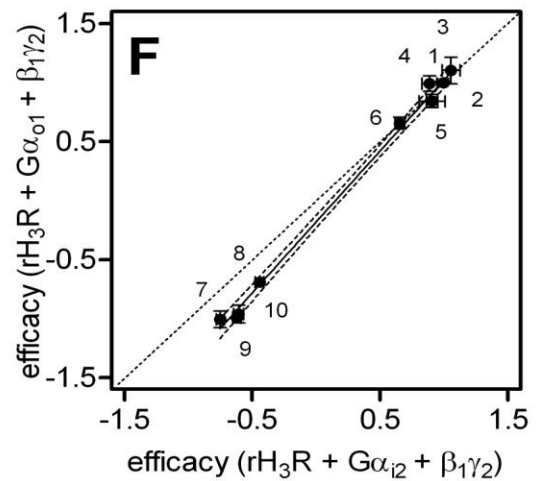
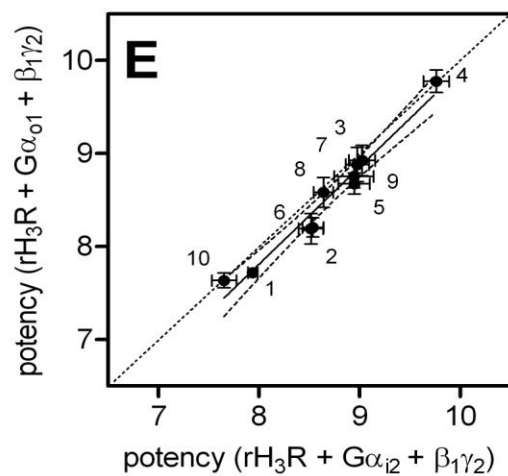
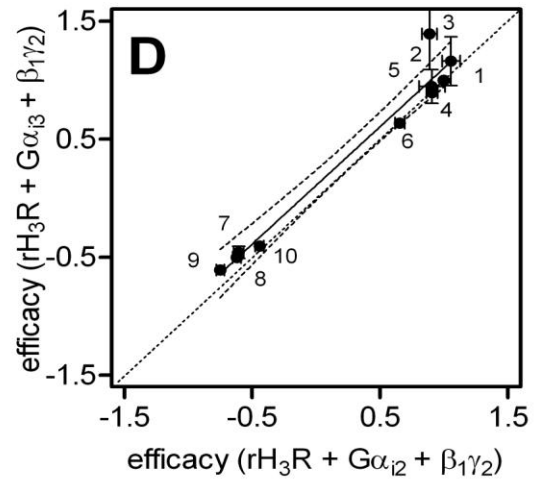
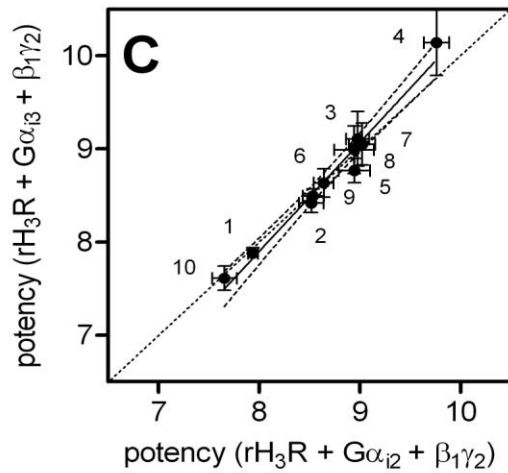
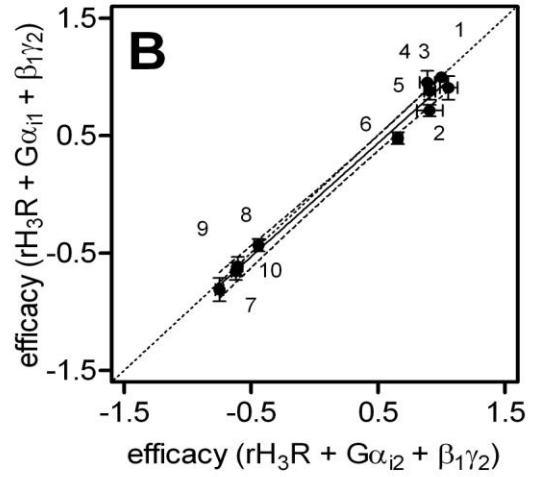
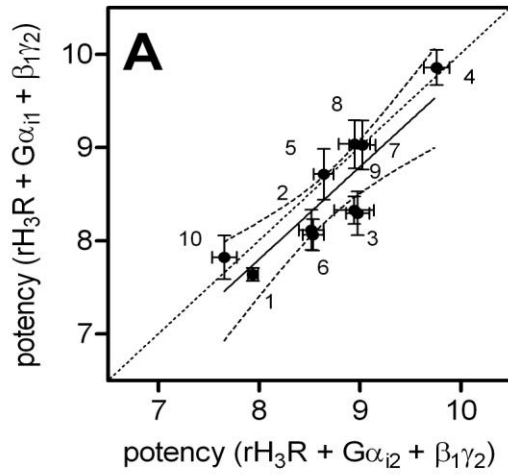


Fig. 7

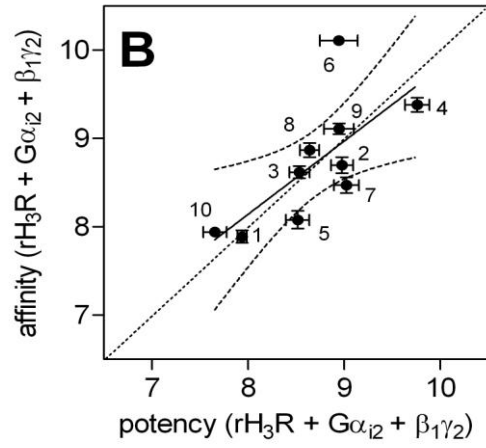
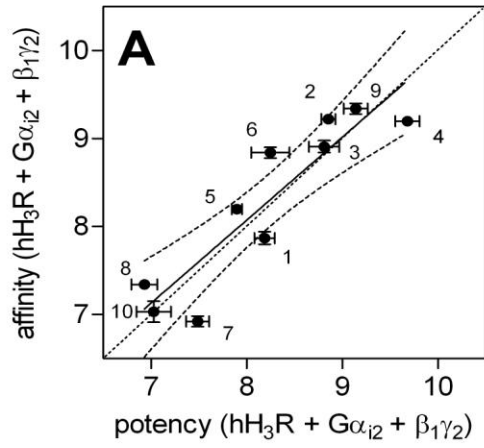
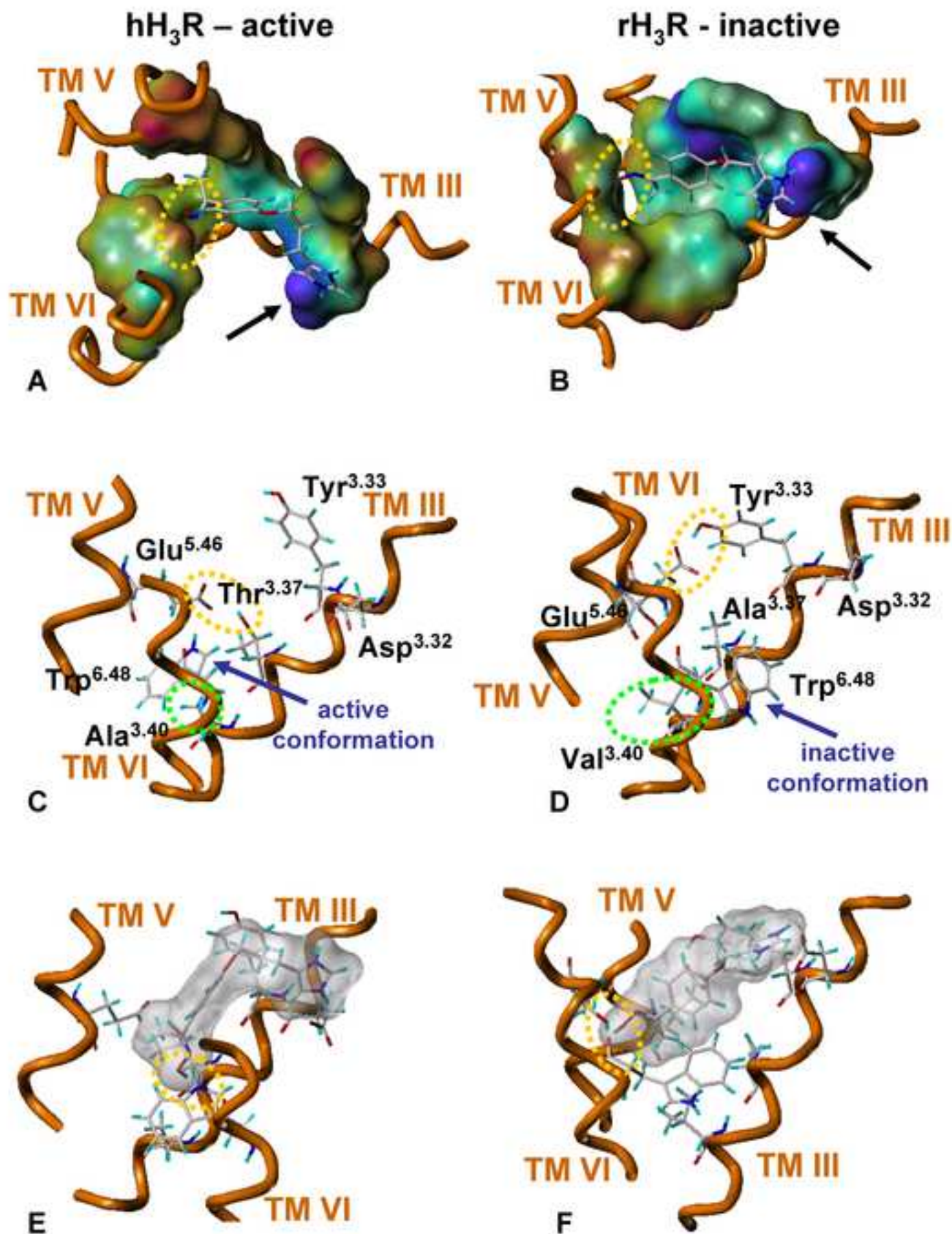
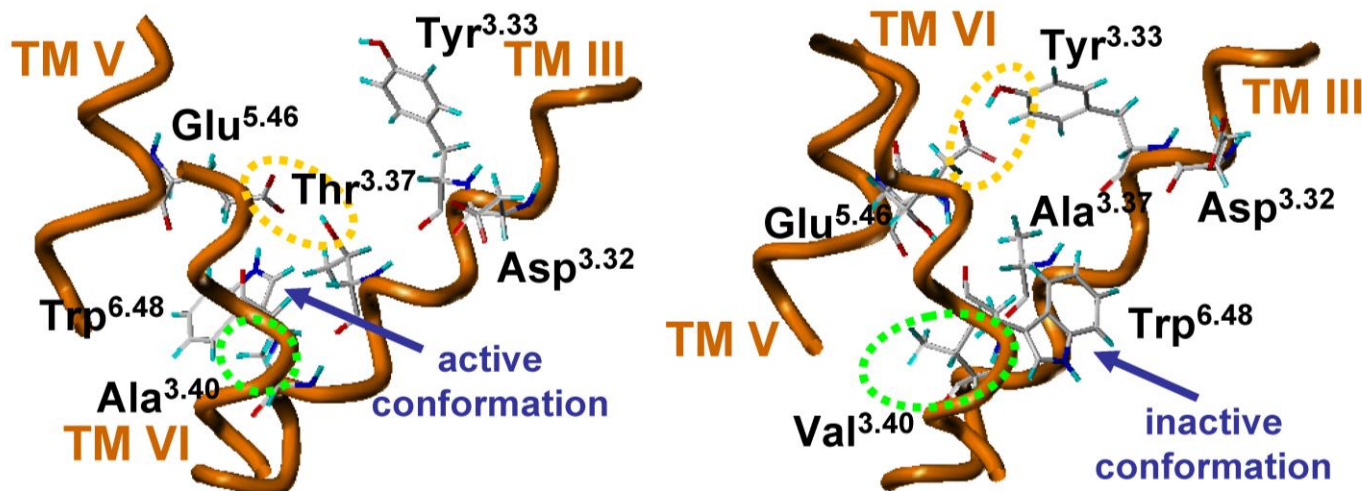


Fig. 8



Graphical Abstract



This paper documents substantial pharmacological differences between human and rat histamine H₃-receptor. Most strikingly, in human H₃-receptor, imoproxifan stabilizes an active conformation. In rat H₃-receptor, imoproxifan stabilizes an inactive conformation.